Transcriptomic analysis and validation study of key genes and the HIF-1α/HO-1 pathway associated with ferroptosis in neutrophilic asthma

LU LIN[1,2*], ZENGHUA LIAO[1*], YINGHUA LI[3], SHITONG PAN[3], SIHUI WU[1], QI-XIANG SUN[1] and CHAOQIAN LI[1]

[1]Department of Pulmonary and Critical Care Medicine, The First Affiliated Hospital of Guangxi Medical University, Nanning, Guangxi 530021, P.R. China; [2]Department of Pulmonary and Critical Care Medicine, The Fifth Affiliated Hospital of Guangxi Medical University, Nanning, Guangxi 530022, P.R. China; [3]Department of Pulmonary and Critical Care Medicine, The Second Affiliated Hospital of Guangxi Medical University, Nanning, Guangxi 530007, P.R. China

Received February 4, 2024; Accepted June 19, 2024

DOI: 10.3892/etm.2024.12722

Abstract. Ferroptosis, as a unique form of cell death caused by iron overload and lipid peroxidation, is involved in the pathogenesis of various inflammatory diseases of the airways. Inhibition of ferroptosis has become a novel strategy for reducing airway epithelial cell death and improving airway inflammation. The aim of the present study was to analyze and validate the key genes and signaling pathways associated with ferroptosis by bioinformatic methods combined with experimental analyzes *in vitro* and *in vivo* to aid the diagnosis and treatment of neutrophilic asthma. A total of 1,639 differentially expressed genes (DEGs) were identified in the transcriptome dataset. After overlapping with ferroptosis-related genes, 11 differentially expressed ferroptosis-related genes (DE-FRGs) were obtained. A new diagnostic model was constructed by these DE-FRGs from the transcriptome dataset with those from the GSE108417 dataset. The receiver operating characteristic curve analysis indicated that the area under the curve had good diagnostic performance (>0.8). As a result, four key DE-FRGs (CXCL2, HMOX1, IL-6 and SLC7A5) and biological pathway [hypoxia-inducible factor 1 (HIF-1) signaling pathway] associated with ferroptosis in neutrophilic asthma were identified by the bioinformatics analysis combined with experimental validation. The upstream regulatory network of key DE-FRGs and target drugs were predicted and the molecular docking results from screened 37 potential therapeutic drugs revealed that the 13 small-molecule drugs exhibited a higher stable binding to the primary proteins of key DE-FRGs. The results suggested that four key DE-FRGs and the HIF-1α/heme oxygenase 1 pathway associated with ferroptosis have potential as novel markers or targets for the diagnosis or treatment of neutrophilic asthma.

Correspondence to: Professor Chaoqian Li, Department of Pulmonary and Critical Care Medicine, The First Affiliated Hospital of Guangxi Medical University, 6 Shuangyong Road, Nanning, Guangxi 530021, P.R. China
E-mail: lichaoqiangood@163.com

*Contributed equally

Key words: ferroptosis-associated genes, neutrophilic asthma, bioinformatics analysis, hypoxia-inducible factor 1 signaling pathway, molecular docking simulation, diagnostic markers

Introduction

Asthma is a complex chronic respiratory disease characterized by inflammation of the airways. The pathogenesis of asthma involves recruiting various inflammatory cells, including eosinophils, airway epithelial cells, macrophages and neutrophils (1). Suppression of airway inflammation by inhaled glucocorticoids is currently the mainstay of asthma treatment. Despite significant advances in asthma treatment, patients with increased airway neutrophilic infiltration tend to experience more severe symptoms and are resistant to corticosteroid therapy (2). Asthma can be divided into Type 2-high endotype and Type 2-low endotype (containing neutrophilic and paucigranulocytic types) (3). Previous studies have reported that neutrophilic asthma is characterized by airway inflammation caused predominantly by neutrophils infiltration, increased secretion of Th1/Th17 cytokines and heightened susceptibility to pulmonary infections (4,5). However, since neutrophilic asthma is rare in asthma, the development of effective diagnosis and treatment is hampered by its unclear pathogenesis. Consequently, further research should be conducted to investigate the pathogenic mechanisms of neutrophilic asthma and to identify potential therapeutic targets that could be effective in its treatment.

Ferroptosis, originally proposed in 2012, has recently been identified as a new form of cell death (6-9). In contrast to other forms of programmed cell death, ferroptosis maintains the structural integrity of the cell nucleus without accumulation of chromosome edges, condensation, blebbing in the plasma membrane, or formation of apoptotic bodies (10). Excessive iron accumulation within cells, lipid peroxidation and oxidative stress are the key indicators of ferroptosis (11).

In recent years, an increasing amount of research has shown that ferroptosis is closely associated with the pathogenesis of asthma. Tang *et al* (12) demonstrated that inhalation of house dust mites can markedly reduce SLC7A11 and glutathione peroxidase 4 (GPX4) activity in lung tissue of mouse, increase the level of reactive oxygen species (ROS) and lipid peroxidation and then induce ferroptosis. Yang and Shang (13) reported that ferroptosis inhibitors can alleviate airway inflammation by inhibiting iron release and lipid peroxidation in the lung tissue of asthmatic mice. Bao *et al* (14) discovered that Lip-1 can attenuate airway inflammation in neutrophilic asthma by regulating ferroptosis regulator levels (including GPX4, PTGS2 and SLC7A11), resulting in the relief of asthma symptom. Although more and more studies link ferroptosis to the pathogenic mechanisms of asthma, the role of ferroptosis in the pathogenesis of neutrophilic asthma remains to be elucidated.

Hypoxia-inducible factor 1 (HIF-1) is a transcriptional activator that regulates physiological responses and oxygen homeostasis when exposed to hypoxic conditions. HIF-1α, one of the HIF subunits, is an essential component of the HIF-1 signaling pathway (15,16). Fu and Zhang (17) indicated that the HIF-1α signaling pathway may be associated with the progression of chronic obstructive pulmonary disease. When HIF-1α accumulates in low-oxygen environments, it moves towards the nucleus, where it binds to hypoxia-responsive elements and stimulates transcription of associated genes in response to cell ischemia and hypoxia. The HIF-1 signaling pathway and related genes play an important role in ferroptosis of other diseases (18). The role of HIF in ferroptosis might exist difference in different diseases and whether HIF-1α was involved in ferroptosis of neutrophilic asthma remains unclear.

The aim of the present study was to elucidate the role of ferroptosis-related key genes and the HIF-1 signaling pathway in the pathophysiology of neutrophilic asthma through bioinformatics analysis and *in vivo* experiments. The association between ferroptosis and neutrophilic asthma was confirmed and the differentially expressed key genes and signaling pathways associated with ferroptosis were identified. The small-molecule drugs that may protect against neutrophilic asthma by preventing ferroptosis were predicted. By screening the key genes and signaling pathways associated with ferroptosis, the present study deepens the understanding of ferroptosis involved in the pathogenesis of neutrophilic asthma and provides a theoretical basis for the diagnosis and treatment of neutrophilic asthma.

Materials and methods

Experimental mice. A total of 12, 4-6-week-old, female BALB/c mice (weight, 18-20 g) were provided by Changsha Tianqin Biotechnology Co., Ltd. The mice were maintained in a special pathogen-free (SPF) laboratory environment and were *free* to drink water and eat food at an ambient temperature of ~23˚C and a humidity of 40-50%. The present study was approved by the Ethics Committee of Guangxi Medical University (approval no. 202210101), the experimental process strictly adhered to the Guidelines for the Care and Use of Laboratory Animals issued by the Ministry of Science and Technology of the People's Republic of China (19).

Mouse model with neutrophil-dominated airway inflammation construction. The experimental mice were randomized into two groups: control (Con), neutrophilic asthma (Neu), each consisting of six mice. The Neu group was sensitized by subcutaneous injection of ovalbumin (20 μg; OVA), complete Freund's adjuvant (75 μl; CFA) and phosphate-buffered saline (25 μl; PBS) on the first day. Subsequently, OVA was diluted into a 1% OVA aerosol solution with sterile PBS dilution and mice were placed in a confined space ~20x30x20 cm in size and aerosolized with 1% OVA using an ultrasonic nebulizer in the closed chamber for 30 min each day (days 22-24). The Con group was sensitized and challenged with PBS. The aforementioned mouse model of neutrophil-dominated airway inflammation was constructed according to previous literature (20,21).

Airway responsiveness testing. Airway responsiveness was assessed 12 h after the last challenge using a previously established method according to our research group (22). After acclimatization for 5 min the laboratory, each mouse was exposed to methacholine (MCh; MilliporeSigma) at different concentrations (PBS, 6.25, 12.5, and 25 mg/ml) for 3 min each. Specific airway resistance (sRaw) was used to indicate airway responsiveness.

Cells count and cytokine detection of bronchoalveolar lavage fluid. According to previous literature (23), after 24 h of the final challenge, mice were anesthetized by intraperitoneal injection of 50 mg/kg 0.3% sodium pentobarbital and, after several minutes of immobility and no response to gentle stimulation, the mice were sacrificed by cervical dislocation. Specifically, the characteristics with cessation of breathing, dilated pupils and cardiac arrest in mice were confirmed as mortality. The behaviors (such as shortness of breath, restlessness and scratching of the mouth, nose and feet) in mice were observed and recorded during the artificial period of the neutrophil-dominated airway inflammation mouse model. The observation period for the model mice was 25 days. Then, the sacrificed mice were used to collect alveolar lavage fluid under endotracheal intubation. After ligation of one side of the trachea, the bilateral lungs were flushed three times with 0.5 ml of cold PBS through the unligated trachea. Bronchoalveolar lavage fluid (BALF) was collected by centrifugation at 400 x g for 10 min at 4˚C. After resuspension of isolated cells in PBS, cells were counted with a hemocytometer and sorted with Wright-Giemsa staining solution (Beijing Solarbio Science & Technology Co., Ltd.) at room temperature for 10 min to calculate different cell proportions. Enzyme-linked immunosorbent assay (ELISA) kits were used to measure IL-17A (cat. no. SEA063Mu; Cloud-Clone Corp.) and interferon-γ (IFN-γ) levels (cat. no. SEA049Mu; Cloud-Clone Corp.) Measure-specific protocols in BALF were as follows.

Pathological staining and immunofluorescence of lung tissue. After fixation with 4% paraformaldehyde for 12 h at room temperature, the left lung tissue was subjected to paraffin embedding with different concentrations of alcohol and xylene, and then cut into 3-μm sections. Subsequently, the obtained samples were stained with hematoxylin-eosin (HE) for 3 min and periodic acid-Schiff (PAS) for 15 min at room temperature

to assess inflammatory cell infiltration and goblet cell proliferation and release, respectively. The percentage of goblet cells staining positive for PAS was scored using a semiquantitative scoring system (0-4 points; none, few, one circle, 2-4 circles and deep ring of inflammatory cell infiltration, respectively) (24). Goblet cell hyperplasia and mucus production were identified by PAS staining. The proportion of goblet cells positive for PAS staining was assessed using a semi-quantitative scoring system. 0 points for no goblet cells detected, 25-50% goblet cells detected, 2 points with 3 points representing 50-75% of goblet cells detected. More than 75% detected goblet cells scored 4 points (25). Immunohistochemical staining was used to detect the expression of neutrophil marker and then further assess neutrophil infiltration in lung tissue (26). The steps of the immunostaining procedure were as follows: First, the paraffin sections were dewaxed into water, then 20X Tris-EDTA antigen retrieval solution (pH 9.0) was used for antigen retrieval solution for 20 min. After blocking endogenous peroxidase activity for 25 min at room temperature with 3% hydrogen peroxide, sections were blocked with 3% BSA (cat. no. GC305010; Wuhan Servicebio Technology Co., Ltd.) for 30 min at room temperature. After shaking off the blocking solution, the sections were covered with Ly6G (cat. no. GB11229; 1:500) and myeloperoxidase (MPO; cat. no. GB12224; 1:1,000) (both Wuhan Servicebio Technology Co., Ltd.) prepared in PBS. The sections were placed flat in a moistened box and incubated at 4˚C overnight. The tissue was then covered separately with HRP-labeled goat anti-rabbit IgG (cat. no. GB23303; 1:200) and goat anti-mouse IgG (cat. no. GB23301; 1:200) (both Wuhan Servicebio Technology Co., Ltd.) and then incubated for 50 min at room temperature. Freshly prepared chromogenic DAB solution (cat. no. G1212; Wuhan Servicebio Technology Co., Ltd.) was used for the chromogenic DAB reaction. After hematoxylin counterstaining for 3 min at room temperature, each section was dehydrated, mounted and observed under a white light microscope.

RNA-Seq data analysis. For mRNA sequencing, lung tissues were collected from three mice in each group. The starting material for RNA sample preparation was 1 μg of lung tissue RNA. Illumina HiSeq 2500/4000 (Gene Denovo Biotechnology Co., Ltd.) was used for sequencing of the RNA library. Transcript reconstruction was performed using Stringtie v1.3.1 (27,28). Gene concentrations in each sample were calculated using RSEM (27). The distance relationship of the samples was examined using principal component analysis (PCA). Differentially expressed genes (DEGs) were identified using the R package DESeq2 (version 1.30.1) (29) of R software (version 4.0.3,http://rproject.org/) (29) at screening thresholds of $P<0.05$ and $|logFC|>1$. The cluster profile package was applied in the Gene Ontology (GO) and Kyoto Encyclopedia of Genes and Genomes (KEGG) analysis (30,31) with $P<0.05$, which corresponds to the significance threshold. To avoid biases arising from the exclusive use of crossover gene enrichment, Gene Set Enrichment Analysis (GSEA) was applied (30) according to the gene expression profile to examine the differences in biological processes between the different groups. The Omicsmart platform (http://www.omicsmart.com) was used for all bioinformatic analyses. The enrichment results were visualized in the form of bubble diagrams.

Screening and biological function analysis of differentially expressed (DE)-ferroptosis-related genes (FRGs). FRGs were obtained from the FerrDB database (http://zhounan.org/ferrdb) and two datasets (GSE143303 and GSE108417) were obtained from the Gene Expression Omnibus database (GEO) (https://www.ncbi.nlm.nih.gov/geo/). The GSE108417 dataset included lung tissue from three healthy mice and three house dust mite-sensitized neutrophilic asthma mouse models. The GSE143303 dataset, on the other hand, consisted of bronchial biopsies from 13 healthy individuals, nine patients with neutrophilic asthma and 38 patients with non-neutrophilic asthma (22 eosinophilic and 16 paucigranulocytic asthma). DEGs analysis was performed using the GEO2R online approach, which was considered significant at $P<0.05$ and $|logFC|>0$. DE-FRGs were identified using the R4.2.3 package Venn (version 1.11) (32). KEGG pathway analysis was performed on the KOBAS 3.0 platform (http://kobas.cbi.pku.edu.cn/). The Pathview website (https://pathview.uncc.edu/analysis) was used to create a graphical representation of the pathway.

Screening and verification of key DE-FRGs. To identify the common DE-FRGs in different neutrophilic asthma mouse models, the R package Venn was used to intersect FRGs with DEGs from RNA-seq analysis and dataset GSE108417. The shared DE-FRGs were then used to construct protein-protein interaction networks (PPIs) using the STRING database (33) (version 12.0; https://string-db.org/) with a pooled score threshold of 0.4. The most important DE-FRGs were then identified. The limma (version 3.54.2) (34) and ggpubr (version 0.6.0) (35) packages were used to evaluate these key DE-FRGs based on the external validation set GSE143303. Furthermore, the receiver operating characteristic (ROC) curve of the model was drawn and the area under the curve (AUC) values were determined using the validation set and R package pROC (version 1.18.0) (36).

Immune infiltration analysis of key DE-FRGs. The GSEA package was used to determine immune cell infiltration levels in lung tissue from mice with neutrophilic asthma and bronchial biopsies from patients with neutrophilic asthma. The proportion of immune cell infiltration was visualized using the ggplot2 (version 3.4.2) (37) R-package accumulation histogram. Furthermore, the relationship between DE-FRGs and infiltrating immune cells was examined using Spearman's rank correlation.

Transcription factor and ceRNA network prediction. The online database TRRUST (version2) (https://www.grnpedia.org/trust/) was used to predict transcription factors for key DE-FRGs. Regulatory networks between key genes and transcription factors were established using Cytoscape (version 3.8.2) (38). TargetScan (version 8.0, http://www.targetscan.org), miRDB (version 6.0) (39) and the miRWalk (version 3) (40) database were used for miRNA prediction of these key DE-FRGs. Subsequently, the Spongescan database (http://spongescan.rc.ufl.edu/) (41) was used to predict the long non-coding (lnc)RNAs that interacted with miRNA and Cytoscape was used to construct and visualize the competing endogenous (ce)RNA network.

Target drug prediction and molecular docking. A comprehensive database developed by DSigDB (http://tanlab.ucdenver.edu/DSigDB) can be used to identify targeted drugs associated with DEGs (42). The present study used the DSigDB website to predict potential drug target associated with key DE-FRGs. The predicted results were imported into Cytoscape software to construct and visualize the protein-drug interaction network. Molecular docking simulation was performed using AutoDock Tool 1.5.7 (43) to clarify the interaction between therapeutic target drugs and their corresponding protein structures of target genes. Targeted therapeutics were downloaded from the DrugBank database (version 5; https://go.drugbank.com/) (44). The PDB profiles of the target proteins were retrieved from the RCSB Protein Data Bank (https://www.rcsb.org/) (45). Analysis and visualization of the docking results were rendered by PyMOL Molecular Graphics System (version 4.6) (46).

Transmission electron microscopy. Lung tissues from mice was preserved and kept in 3% glutaraldehyde at 4˚C. After fixation in 1% osmium tetroxide for 2 h, the tissues were subjected to gradient ethanol dehydration and epoxy resin embedding. Ultrathin sections (60-90 nm) were prepared and stained with uranyl acetate and lead citrate. Finally, a JEM-1400FLASH transmission electron microscope (JEOL, Ltd.) was used to observe the morphology of mouse bronchial epithelial cells.

Determination characteristics of ferroptosis in lung tissue. To further demonstrate the occurrence of ferroptosis in neutrophilic asthma, the expression of malondialdehyde (MDA) and reduced glutathione (GSH) in lung tissues of mice was examined. Lung tissue was processed into lung homogenate using a tissue homogenizer according to the reagent instructions. The total protein concentration was determined using the Enhanced BCA Protein Assay Kit (cat. no. P0010S; Beyotime Institute of Biotechnology). The MDA and GSH contents were detected according to the instructions of the MDA kit (cat. no. A003-1; Nanjing Jiancheng Bioengineering Institute) and the GSH and GSSG Assay Kit (cat. no. S0053; Beyotime Institute of Biotechnology), respectively.

Reverse transcription-quantitative (RT-q) PCR. TRIzol® (Invitrogen; Thermo Fisher Scientific, Inc.) was used to extract total tissue RNAs. A reverse transcription kit (Takara Bio, Inc.) was used for reverse transcription. Subsequently, TB Green® Premix Ex Taq™ II (Takara Bio, Inc.) was utilized for the implementation of qPCR. Real-time PCR was performed on a 7500 Real-Time PCR System (Applied Biosystems). The following PCR cycling parameters were adopted for amplification: 95˚C for 30 sec, then 40 cycles of denaturation at 95˚C for 3 sec, and annealing and extension at 60˚C for 30 sec. Glyceraldehyde-3-phosphate dehydrogenase (GAPDH) expression was used to normalize the amplified products. All the procedures were performed according to the manufacturers' protocols. Additionally, the $2^{-\Delta\Delta Cq}$ method and real-time quantitative PCR were used to analyze relative gene expression data in order to determine the relative expression levels (fold-change) (47). These experiments were replicated three times. Primer sequences were designed and synthesized by China Gensys Biotechnology Co., Ltd. and the Beijing TsingKe Biological Technology Company (Table SI).

Western blotting. Total proteins from lung tissue were extracted with RIPA buffer (Beijing Solarbio Science & Technology Co., Ltd.). The protein content was measured using a BCA kit (Beyotime Institute of Biotechnology). Soluble protein (40 μg) was added to each lane, and 10 and 12.5% gels were used for SDS-PAGE. Next protein imprinting to a PVDF membrane was achieved by using Invitrolon polyvinylidene fluoride filter paper. The membranes were blocked with 5% defatted milk in TBST (1% Tween-20) solution for 1-1.5 h at room temperature. Subsequently, Primary antibodies against HIF-1α (cat. no. 340462; 1:1,000; Zenbio), heme oxygenase 1 (HO-1; Abmart, TA5393; 1:1,000) and GPX4 (cat. no. T56959; 1:1,000; Abmart) were then added and incubated overnight at 4˚C. After washing three times with 1X TBST, the membranes were incubated with a goat anti-rabbit IgG H&L secondary antibody (cat. no. bs-0295G; 1:10,000; BIOSS) for 60-90 min at room temperature. After washing with TBST three times in the dark, an Odyssey system (LI-COR Biosciences) was used for protein band detection. The proteins were analyzed and visualized using ImageJ software (National Institutes of Health).

Statistical analysis. GraphPad Prism 9.0.0 software (Dotmatics) was adopted for statistical analysis. The Shapiro-Wilk test was performed to examine whether the measured data were normally distributed. Results between groups were compared by independent t-test or K-W test and expressed as mean ± standard deviation (SD). One-way ANOVA was performed after the normality test and post hoc LSD was performed to distinguish differences between groups. Data conforming to abnormal distribution were compared by Mann-Whitney U test. $P<0.05$ was considered to indicate a statistically significant difference.

Results

Mice with neutrophil-dominated airway inflammation induced by OVA and CFA. Fig. 1 displays the schematic diagram of this study. Fig. 2A shows the established asthma mouse model with neutrophil-dominated airway inflammation induced by OVA in combination with CFA. It can be seen that the specific airway resistance (sRaw) in mice increased with the increased dose of nebulized methacholine in Pulmonary function tests. After inhalation of Mch aerosol at different doses (6/12.5/25 mg/ml), the Neu group exhibited significant airway hyperresponsiveness compared with the Con group in Fig. 2B. In addition, the total number of cells in BALF and the proportion of neutrophils were markedly increased in the Neu group compared with the Con group (Fig. 2C and D). As shown in HE staining, there was greater infiltration of inflammatory cells around the airways, mucus secretion and goblet cell proliferation than the control group (Fig. 2E and F). The PAS staining results (Fig. 2E and G) of the Neu group also showed greater airway inflammation compared with the Con group. Furthermore, significantly increased expression of neutrophil markers for Ly6G and MPO can be found in the lung tissue of neutrophilic asthma mice compared with the Con group (Fig. 2H-J). According to ELISA results, IL-17A and IFN-γ cytokines in the BALF of neutrophilic asthmatic mice were significantly higher compared with those

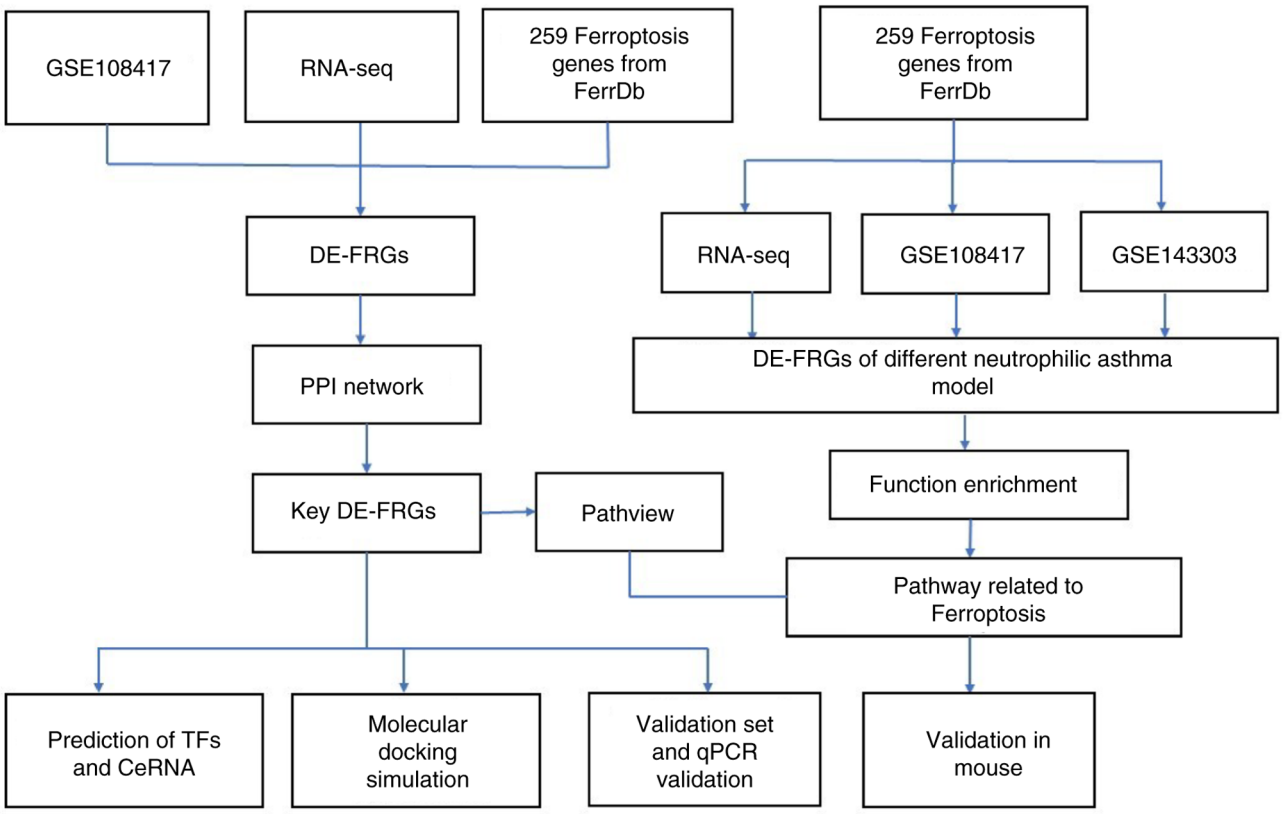

Figure 1. Schematic diagram of the present study.

in the control group (Fig. 2K and L). Previous studies (48,49) reported that overexpression of IFN-γ and IL-17A, as a common phenotype in severe asthma, is closely associated with airway neutrophil infiltration and poor response to corticosteroids. The results in Fig. 2 showed that an asthma mouse model with the typical feature of neutrophilic inflammation was successfully established.

Identification and functional enrichment analysis of DEGs based on RNA-seq data. RNA-seq data were obtained and read length count values (RPKM) were normalized. The difference between the control and asthma groups can be effectively distinguished from Fig. 3A by PCA data with good quality. A total of 1,639 DEGs were identified. The top 50 DEGs are depicted in the heatmap (Fig. 3B), while the volcano plot shows all DEGs (Fig. 3C). GO enrichment analysis in Fig. 3D showed that the most abundant DEGs were clearly associated with immune-related biological processes, such as immune system, immune response and inflammatory response. KEGG pathway analysis revealed that the NF-kB, Th17, Th1 and Th2 cell differentiation and chemokine signaling pathways were the main pathways involved (Fig. 3E). In addition, GSEA showed that biological processes, such as IFN-γ production, activation of an immune response and signaling pathways (including NF-kB, NOD-like receptor and HIF-1) are also associated with the pathogenesis of neutrophilic asthma (Fig. 3F and G).

DE-FRGs and biological functions analysis. To obtain DE-FRGs in different neutrophilic asthma models, 259 FRGs from the FerrDB database were used to intersect with RNA-sequencing data, GSE108417 and GSE143303, separately (Fig. 4A-C). Simultaneously, KEGG enrichment of DE-FRGs was performed in three datasets using the online KOBAS tool. The analysis revealed that ferroptosis, HIF-1, NOD-like receptor and IL-17 signaling pathways were enriched in the three neutrophilic asthma models (Fig. 4D-I; Tables SII-SIV). It can be hypothesized that these signaling pathways may be closely associated with the progression of ferroptosis in neutrophilic asthma. According to the DE-FRGs identified in the GSE143303 dataset and the RNA-Seq data, the ferroptosis pathway (Fig. 5A and C) and the HIF-1 pathway (Fig. 5B and D) were mediated Pathview mapped. Several DE-FRGs have been found to be associated with ferroptosis. Furthermore, it can be seen from both the GSE143303 dataset and the RNA-seq dataset that HIF-1 exerts an important influence on ferroptosis through the modulation of HMOX1.

Screening and verification of key ferroptosis-related differential genes. By intersecting DE-FRGs from the transcriptome dataset with those from the GSE108417 dataset, 11 key DE-FRGs were identified (Fig. 6A). Among them, eight upregulated and three downregulated genes can be seen in Fig. 6B. Subsequently, correlation analysis revealed that the expression of HMOX1 was positively associated with TNFAIP3 (Fig. 6C). The PPI network in Fig. 6D showed that eight genes involved in ferroptosis have tightly interactive network relationships. As a result, it can be speculated that these key DE-FRGs (IL-6, CXCL2, HMOX1, CD44, SLC7A11, SLC7A5, CAV1 and TNFAIP3) may play an essential role in ferroptosis in mice with neutrophilic asthma.

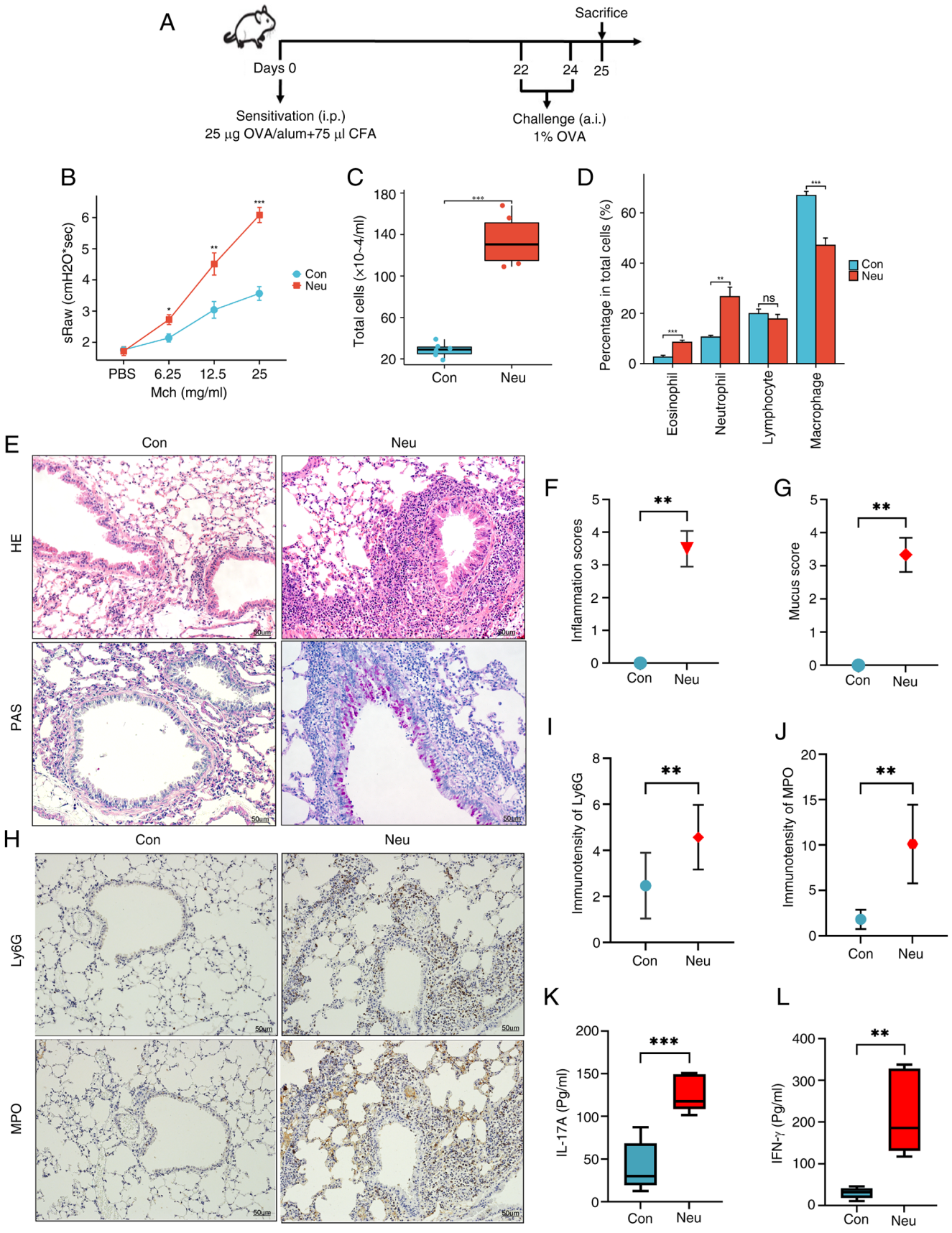

Figure 2. Construction of the neutrophilic asthma mouse model. (A) Model construction protocol. (B) sRaw stimulated by different doses of Mch (mg/ml); (C) Total number of inflammatory cells in BALF. (D) Percentages of different types of cells in BALF; (E) Lung tissues were stained with HE and PAS. (F) HE inflammation score. (G) PAS-positive fraction. Magnification, x200. (H) IHC was used to observe the expression of neutrophil markers Ly6G and MPO in lung tissue of mice; Magnification, x200 (blue refers to the nucleus, brown is the marker protein). (I) Expression of LY6G in lung tissue. (J) Expression of MPO in lung tissue. (K and L) IFN-γ and IL-17A secretion within BALF (n=6). Statistical significance vs. the control group is indicated (*P<0.05, **P<0.01 and ***P<0.005). sRaw, specific airway resistance Mch, methacholine; BALF, bronchoalveolar lavage fluid; HE, hematoxylin-eosin; PAS, periodic acid-Schiff; IHC, immunohistochemistry; Con, Control; Neu, neutrophilic asthma.

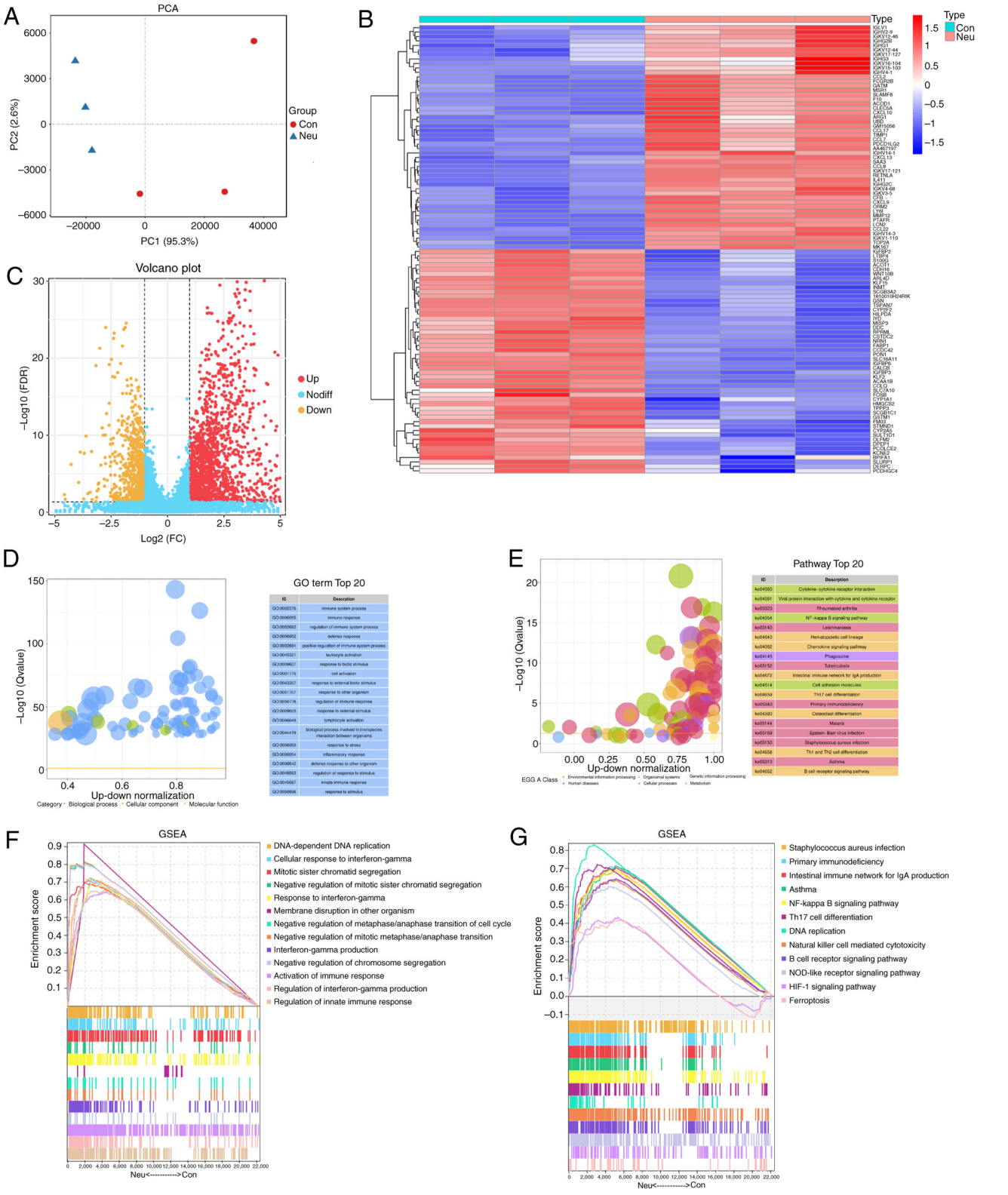

Figure 3. Identification and enrichment analysis of DEGs. (A) PCA plot showing clustering of control samples (yellow) and Neu samples (blue). (B) Heatmap of DEGs, where red and blue stand for genes with up- and down-regulation, separately. (C) Volcano plot of DEGs, where red and blue stand for genes with up- and down-regulation, separately. (D) GO annotation. (E) KEGG analysis. GSEA of (F) GO terms and (G) KEGG pathways. DEGs, differentially expressed genes; PCA, principal component analysis; Neu, neutrophilic asthma; GO, Gene Ontology; KEGG, Kyoto Encyclopedia of Genes and Genomes; GSEA, Gene Set Enrichment Analysis; Con, Control.

External validation of key DE-FRGs. Based on the validation dataset GSE143303, the present study sought to validate the expression of these key DE-FRGs in bronchial biopsy tissues from patients with neutrophilic asthma. As consequence, the expression of IL6, CXCL2, HMOX1, SLC7A5 and TNFAIP3 was significantly increased in bronchial biopsies from

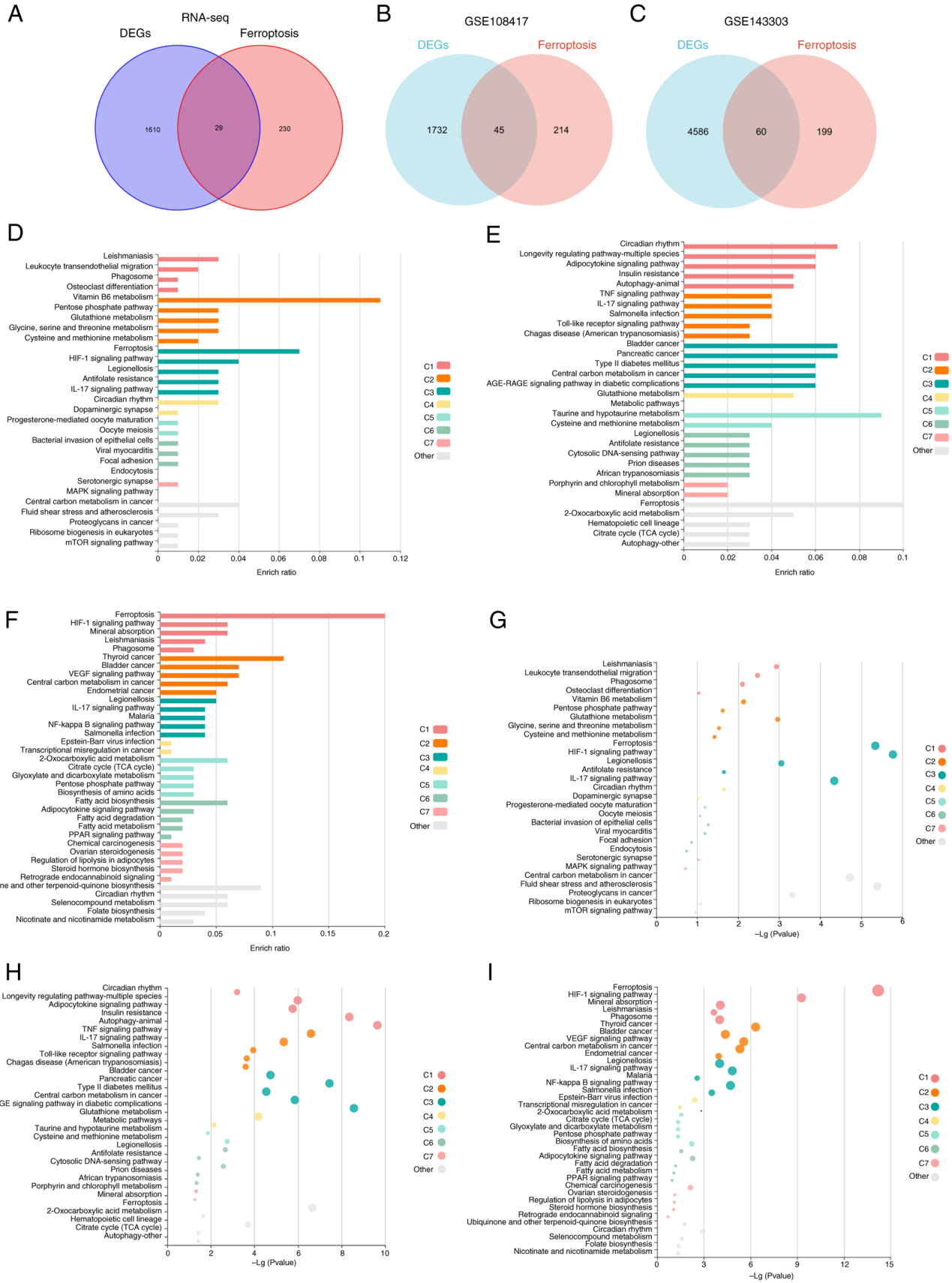

Figure 4. Evaluation of genes associated with ferroptosis. (A) Venn diagram illustrating intersection between DEGs in RNA-seq and genes associated with ferroptosis. (B) Venn diagram depicting the overlap between DEGs and ferroptosis-associated genes in the GSE108417 dataset. (C) Venn diagram demonstrating correlations of DEGs with FRGs in the GSE143303 dataset. (D) KEGG enrichment of DE-FRGs, as derived from RNA-seq data. (E) KEGG enrichment of differential genes implicated in ferroptosis, as found in the GSE108417 dataset. (F) KEGG enrichment of ferroptosis-related differential genes, as obtained from the GSE143303 dataset. (G) Bubble plot visualizing-Log (P-value) based on RNA-seq data. (H) A bubble plot displaying-Log (P-value) of GSE108417 dataset. (I) Bubble chart presenting-Log (P-value) as derived from the GSE143303 dataset. DEGs, differentially expressed genes; RNA-seq, RNA sequencing; FRGs, ferroptosis-related genes; KEGG, Kyoto Encyclopedia of Genes and Genomes; DE, differentially expressed.

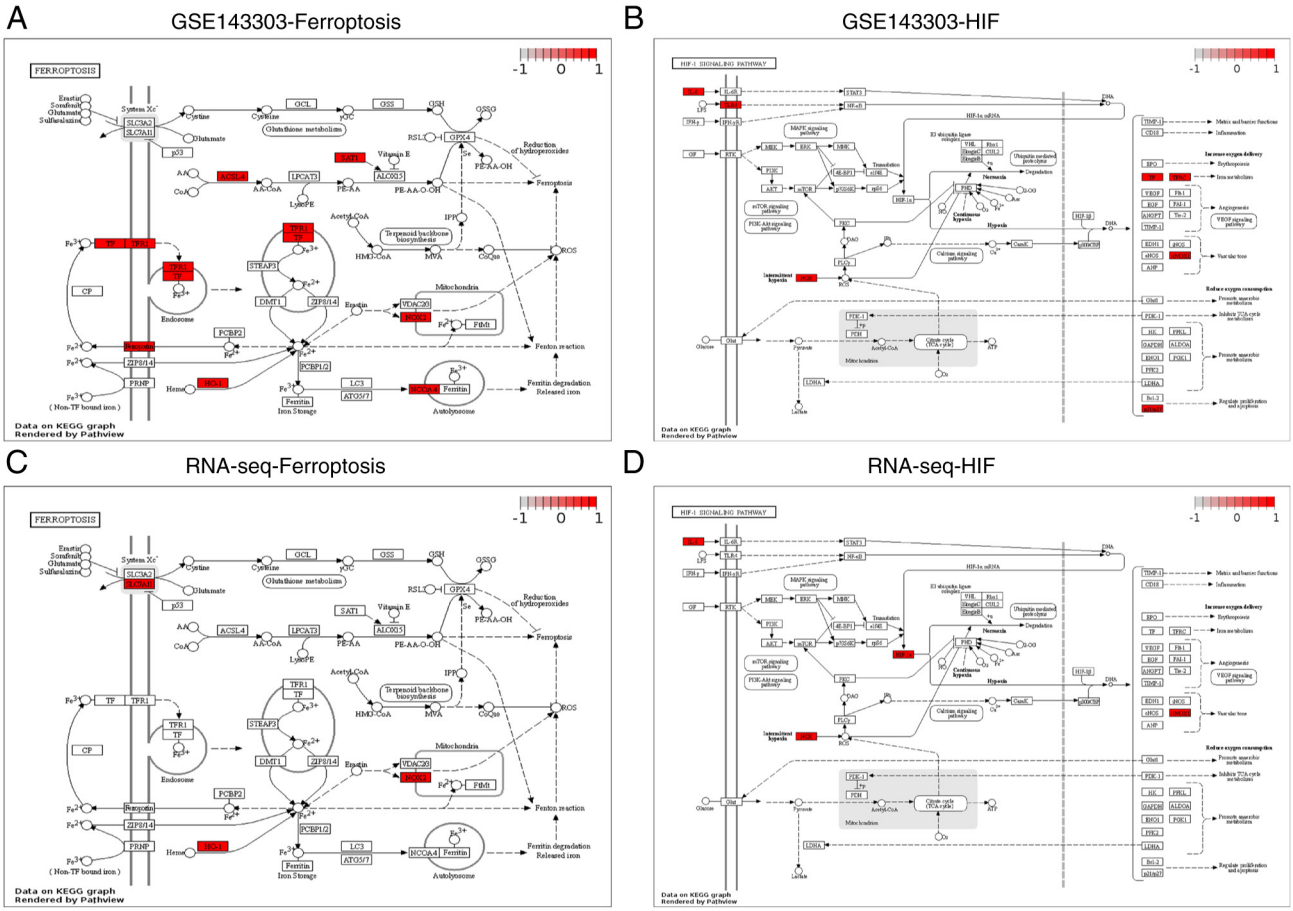

Figure 5. Mapping of KEGG signaling pathways for (A) Ferroptosis and (B) HIF-1, derived from DE-FRGs in GSE143303 dataset. (C) Ferroptosis and (D) HIF-1derived from DE-FRGs in RNA-seq dataset. KEGG, Kyoto Encyclopedia of Genes and Genomes; HIF-1, hypoxia-inducible factor 1; DE-FRGs, differentially expressed ferroptosis-related genes; RNA-seq, RNA sequencing.

neutrophilic asthma compared with normal subjects (P<0.05). There were not clearly significant differences in CD44 and SLC7A11, whereas CAV1 was not detected in this dataset (Fig. 7A). To further investigate the potential of these five DEGs as diagnostic biomarkers in neutrophilic asthma, an ROC curve was constructed. As shown in Fig. 7B, the AUC values of IL6, CXCL2, TNFAIP3, SLC7A5 and HMOX1 were 0.966, 0.923, 0.872, 0.872 and 0.812, respectively, indicating high diagnostic efficacy. It can also be seen from Fig. 7C that the top five DE-FRGs were significantly different between patients with neutrophilic asthma and healthy control participants based on the established logistic regression model and the AUC value (1.000). In addition, the expression results of these genes in normal, neutrophilic and eosinophilic asthma in Fig. 7D-H showed that there were significant differences between patients with neutrophilic (Neu) and eosinophilic asthma (Eos) in the expression of HMOX1, CXCL2, SLC7A5 and IL-6. Collectively, these results suggest that the four DE-FRGs may play an important role in neutrophilic asthma.

Identification of key DE-FRGs in neutrophilic asthma. To verify the bioinformatics analysis, the expression of hub ferroptosis-related differential genes *in vivo* was further examined. The qPCR results showed that the mRNA expression levels of HMOX1, CXCL2, SLC7A5 and IL-6 in the lung tissue of the asthmatic mice (Fig. 7I) were significantly higher than those of the control group. However, the expression level of TNFAIP3 in the lung tissue of asthmatic mice was lower than that of control mice. The results demonstrated the reliability of the bioinformatics analysis.

Analysis of the immune microenvironment in neutrophilic asthma. The present study performed single-sample GSEA (ssGSEA) to understand more clearly the immune microenvironment in neutrophilic asthma and analyzed the correlations between key DE-FRGs and immune cells. It can be found that both the lung tissue of neutrophilic asthmatics mice (Fig. 8A) and the bronchial biopsy tissue of neutrophilic asthmatics patients (Fig. 8B) were associated with various immune cells (including macrophages, neutrophils, Type2 T helper cells, or Type17 T helper cells). In mouse lung tissue, DE-FRGs associated with infiltrating cells without a significant difference (Fig. 8C), possibly due to the small sample size. In human bronchial biopsy tissues, HMOX1 was markedly positively associated with immune cells, such as macrophages, Type1/Type2/Type17 T helper cells, active CD4 T cells and CD8 T cells in central memory. CXCL2 showed a positive relationship with gamma delta T cells. IL-6 showed a significant positive relationship with activated dendritic cells. SLC7A5 had a dramatic positive relationship with gamma delta T cells and a negative relationship with effector CD8 T cells (Fig. 8D). These results further confirmed the involvement of various

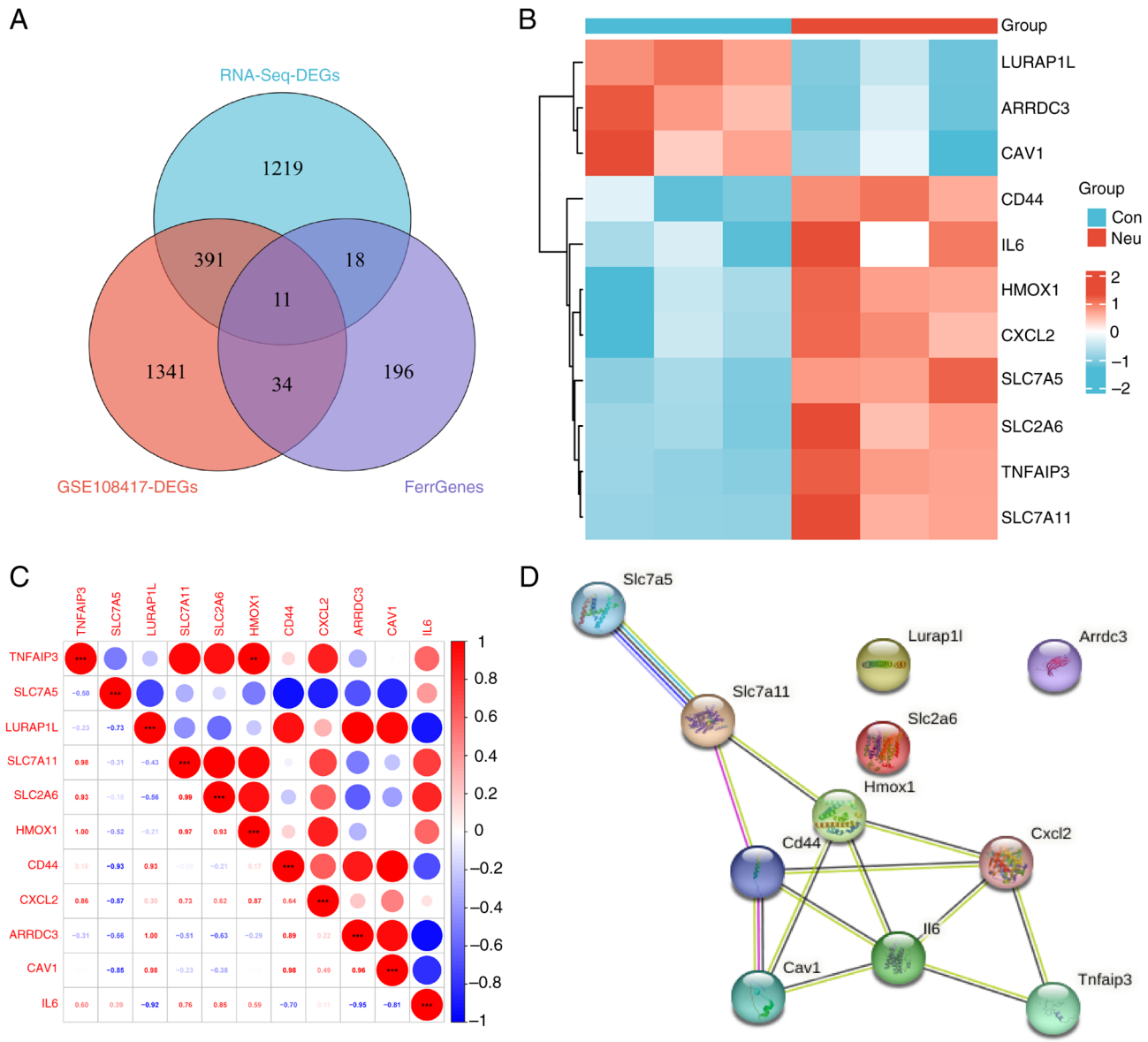

Figure 6. Analysis of ferroptosis-associated genes in neutropenic asthmatic mice. (A) Venn diagram representing the intersection between DEGs from RNA-seq and GSE108417 datasets, with a focus on ferroptosis-related genes. (B) Heatmap depicting ferroptosis-associated genes in neutropenic asthmatic mice. Red and blue stand for genes with up- and downregulation, separately. (C) Correlation analysis of ferroptosis-related genes in neutropenic asthmatic mice. A positive correlation is denoted in red, while a negative correlation is represented in blue. (D) PPI network of key ferroptosis genes in neutrophilic asthma. **P<0.01 and ***P<0.001. DEGs, differentially expressed genes; RNA-seq, RNA sequencing; PPI, protein-protein interaction; Con, Control; Neu, neutrophilic asthma.

immune cells in the progression of neutrophilic asthma and that DE-FRGs are associated with various immune cells.

Prediction of key DE-FRGs transcription factors and CeRNA network construction. To investigate the possible regulation mechanisms of these DE-FRGs at the transcriptional and post-transcriptional levels, transcription factor and ceRNA prediction and network construction were performed. A total of eight transcription factors (TFs) were predicted using the TRRUST online database (https://www.grnpedia.org/trust/). The mRNA-TF network was constructed using Cytoscape, as shown in Fig. 9A. It can be seen that RELA and NF-κB were simultaneously regulated by most major DE-FRGs, suggesting that the two TFs may be involved in ferroptosis in neutrophilic asthma at the transcriptional level. Then, StarBase, miRDB and miRanda databases were used to predict miRNAs that might have regulatory relationships between these genes and a total of 66 miRNAs were predicted. Finally, 75 lncRNAs interacting with these 66 common miRNAs were predicted by the Spongescan database and the ceRNA network of DE-FRGs, miRNAs and lncRNAs was constructed (Fig. 9B).

Drug prediction and molecular docking simulation. The DSigDB database was used to predict the potential therapeutic drugs associated with hub DE-FRGs. As a result, 37 target drugs with potential therapeutic effects were obtained. Among them, there were 25 potential therapeutic drugs associated with key DE-FRGs in IL6. Of these, four small-molecule drugs (SORAFENIB, SUNITINIB, STANNSOPORFIN and ASPIRIN) were found to correlate with HMOX1 and five target drugs (BCG VACCINE, BATIMASTAT, STAUROSPORINE, ALTEPLASE and DEFEROXAMINE) were associated with

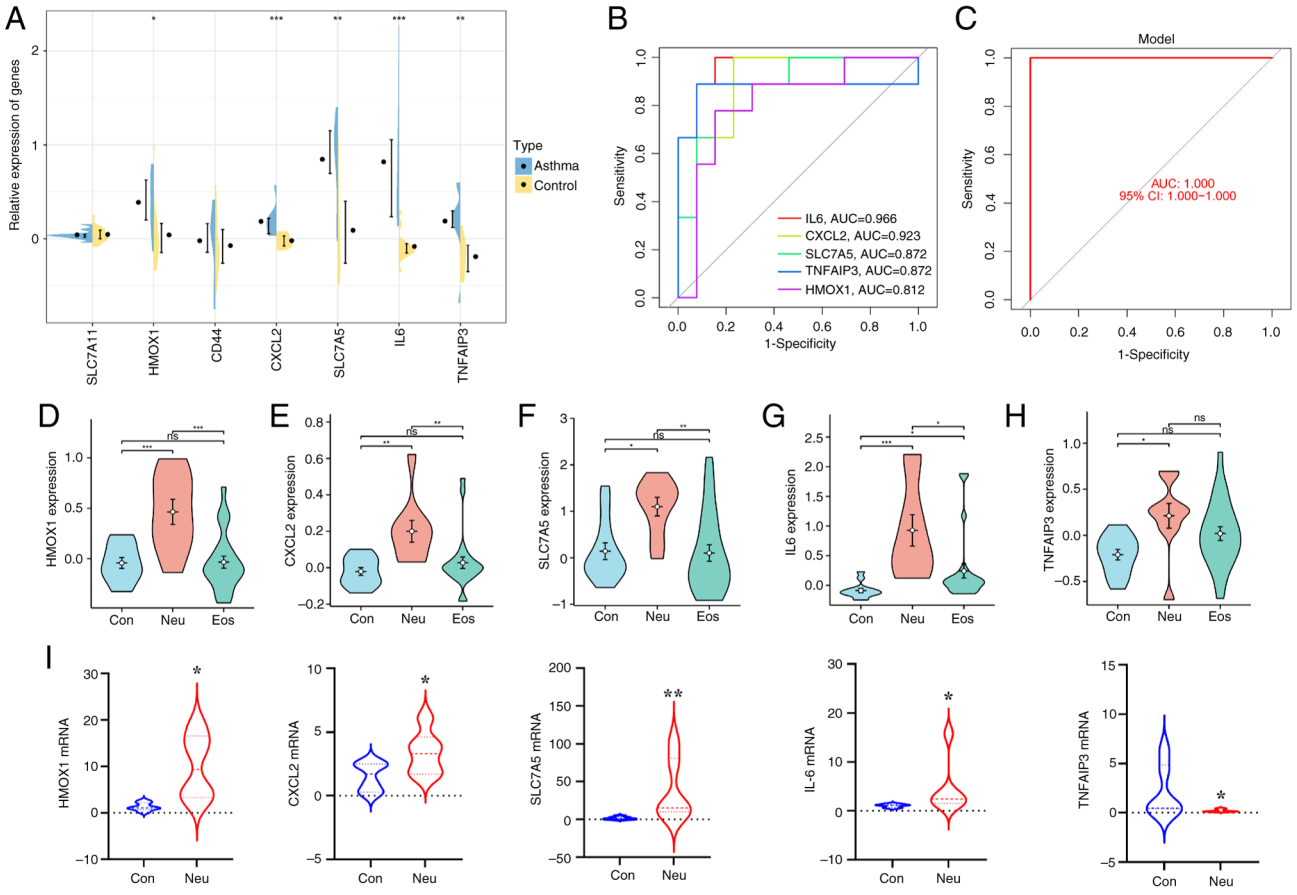

Figure 7. External verification of key DE-FRGs. (A) Comparison of the relative expression levels of hub DE-FRGs of Neu compared with Con groups; the significance level was P<0.05; (B and C) ROC curves of the key DE-FRGs. (D-H) Differences in the expression of key DE-FRGs in neutrophilic asthma and eosinophilic asthma from dataset GSE143303. (I) The mRNA expression levels of hub FRGs within mouse lung tissue. *P<0.05, **P<0.01 and ***P<0.001. DE-FRGs, differentially expressed ferroptosis-related genes; Neu, neutrophilic asthma; Con, Control; ROC, receiver operating characteristic; Eos, eosinophilic asthma; ns, not significant; CI, confidence interval.

CXCL2. In addition, SLC7A5 exists as a (MELPHALAN) protein-drug interaction network. Subsequently, a chemical mRNA network was constructed and visualized using Cytoscape (Fig. 10). Of these target drugs, deferoxamine has been reported in previous studies to inhibit HDM-induced airway inflammation in mice by regulating ferroptosis (50). However, further research was needed to determine clinical effectiveness in patients with asthma. Subsequently, through molecular docking simulations, 35 small molecule drugs that can target ferroptosis-related proteins to exert anti-inflammatory activities in the neutrophilic airways were further studied to explore the molecular interactions between these potential therapeutic agents and the main proteins of neutrophil asthma. Simulated docking results of 13 drugs with a docking score of ≤-6 Kcal/mol are shown in Table I. Fig. 11 also shows that the 2D/3D structural diagrams of seven candidate drug molecules (Sorafenib, Stanannsopofin, Sunitinib, Batimastat, Staurosporine, Levofloxacin and Nelfinavir) and their intermolecular interaction have a lower affinity of ≤-7 Kcal/mol. Four potential therapeutics (Sunitinib, Batimastat, Staurosporine and Nelfinavir) were found to interact with the corresponding primary proteins and had a higher binding affinity energy (≤-8 Kcal/mol). Interestingly, further analysis may reveal that two binding residues (Arg85 and Gly163) were mutual intermolecular interaction sites in the structure of HMOX1, while the Gln24 residue is present in the binding residue on the CXCL2 sequence. Deng *et al* (51) also emphasized that the binding affinity energy (>-6 kcal/mol) triggered high binding affinity of the potential therapeutic drug with the target molecules. Thus, these data showed that 13 drugs had a higher stable binding to proteins.

Validation of HIF-1 pathway associated with ferroptosis in neutrophilic asthma. The significance of the HIF-1 signaling pathway in the development of neutrophilic asthma is confirmed by the aforementioned bioinformatics analyses. The present study then further verified the occurrence of ferroptosis in neutrophilic asthma. Fig. 12A shows the change in mitochondrial morphology in mouse airway epithelial cells. It can be seen that the ciliated epithelial cells of mitochondria morphology in the Neu group exhibited a smaller size and a slightly higher membrane and inner membrane density than those in the Con group, while the cristae of mitochondria morphology were reduced in the Neu group. These features are consistent with those observed in ferroptosis (52). Lipid peroxidation and impaired REDOX responses were further confirmed as important features of ferroptosis. The results in Fig. 12B showed that the MDA concentration in the lung tissue of the Neu group was significantly higher than that of the Con group. The degree of lipid peroxidation is positively

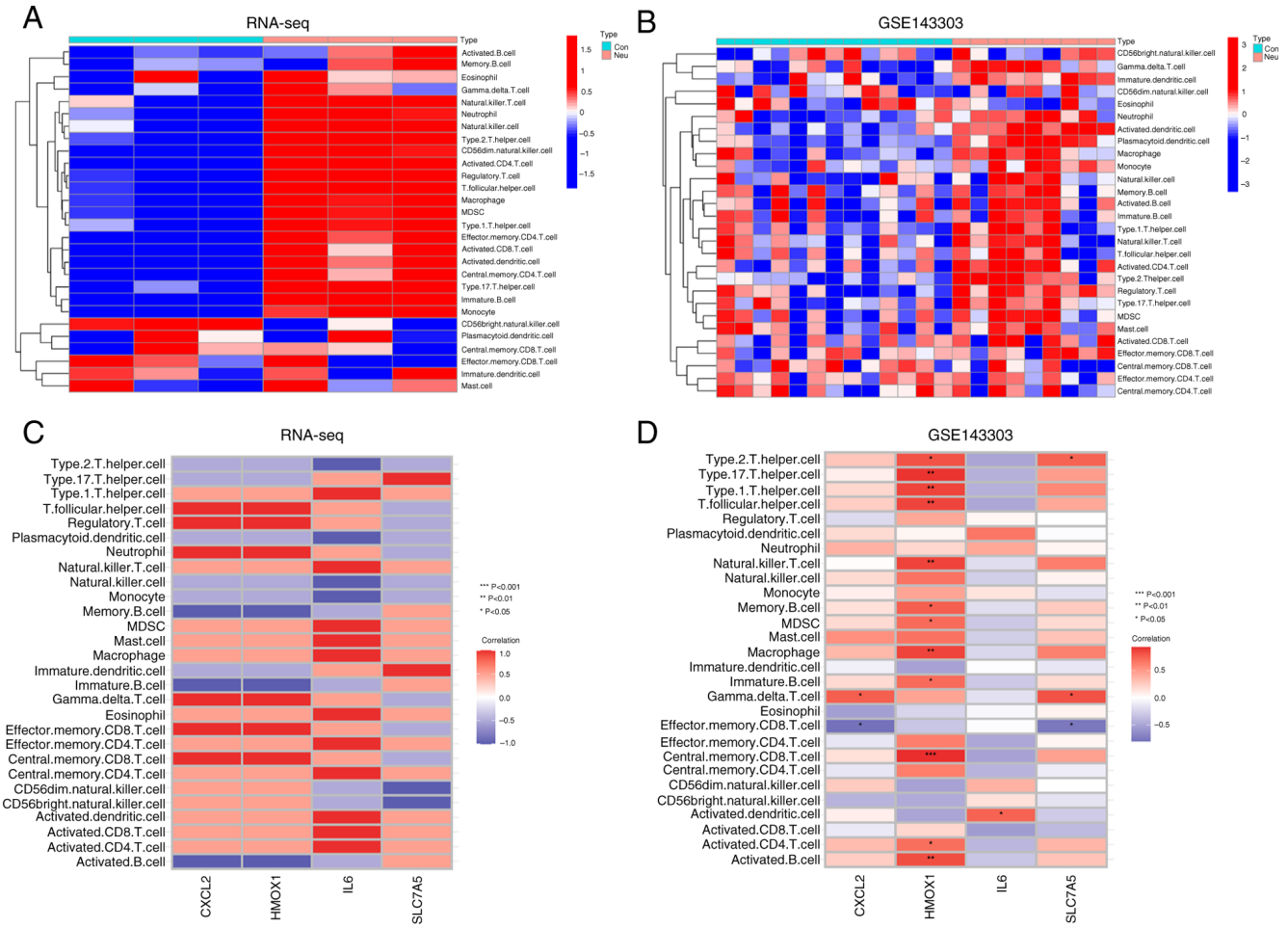

Figure 8. Analysis of immune cell infiltration. (A) Heatmap illustrating ssGSEA of immune infiltration in the lung tissue of mice suffering from neutropenic asthma. (B) Heatmap demonstrating immune cell infiltration in the GSE143303 dataset. (C) Correlation analysis detailing the immune infiltration within lung tissue in neutrophilic asthmatic mice in relation to hub genes differentially expressed in ferroptosis. (D) Correlation study of immune cell infiltration associated with hub genes differentially expressed in ferroptosis within human bronchial biopsy tissue. *P<0.05, **P<0.01 and ***P<0.001. ssGSEA, single-sample GSEA; GSEA, Gene Set Enrichment Analysis; Con, Control; Neu, neutrophilic asthma.

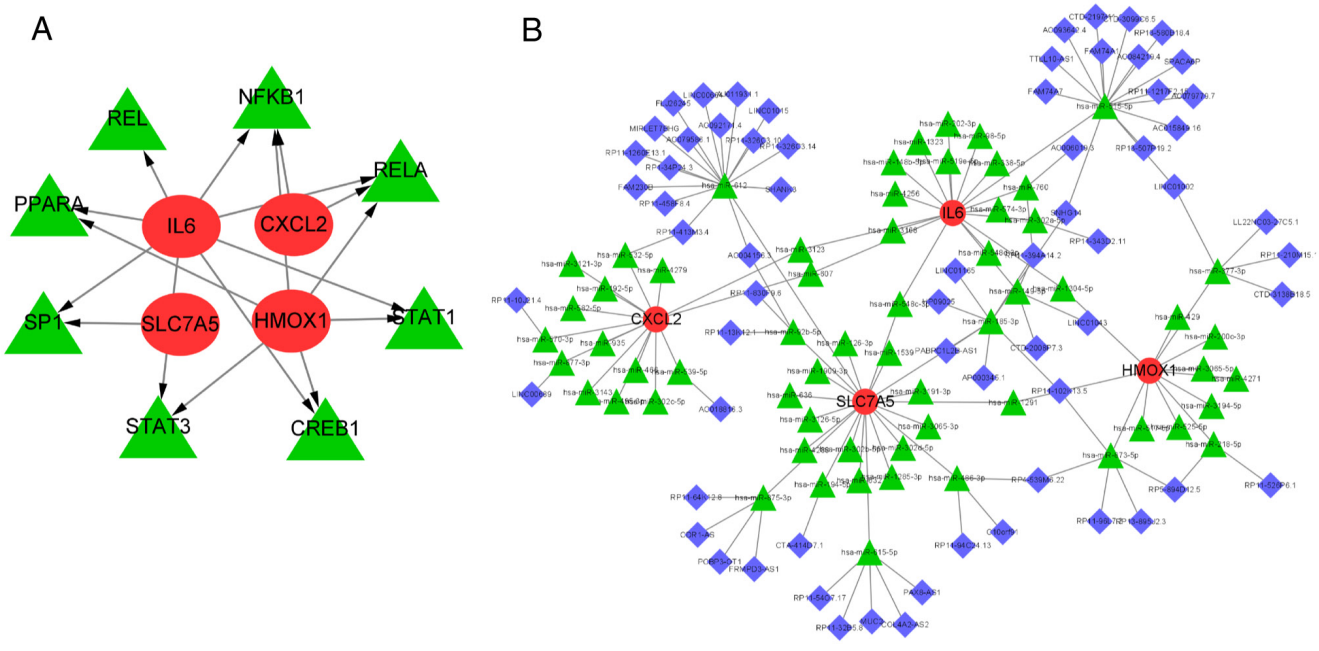

Figure 9. Regulatory network depiction. (A) The network of hub genes and TFs (Red circles signify hub genes associated with ferroptosis, while yellow triangles denote TFs). (B) competing endogenous RNA regulatory network. TFs, transcription factors.

Table I. Docking score (≤-6 kcal/mol) of 13 potential therapeutic drugs in which they combined with the primary proteins in neutrophilic asthma.

Primary proteins	HMOX1 (Kcal/mol)	CXCL2 (Kcal/mol)	IL6 (Kcal/mol)
Potential therapeutic agents	Sorafenib (-8.8), Stanannsopofin (-7.4), Sunitinb (-7.1)	Batimastat (-8.9), Deferoxamine (-6.3), Staurosporine (-8.4)	Fenofibrate (-6.8), Fentanyl (-6.8), Gemfibrozil (-6.5), Ibudilast (-6.1), Levofloxacin (-7.5), Linezolid (-6.8), Nelfinavir (-8.2)

HMOX1, heme oxygenase 1; CXCL2, chemokine ligand 2.

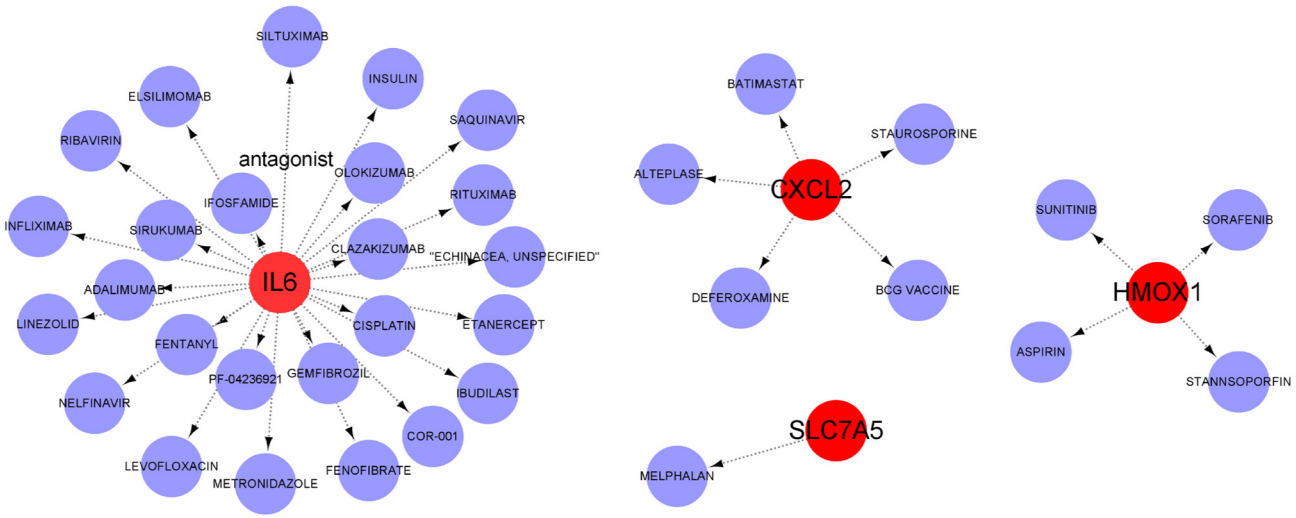

Figure 10. Drug prediction. Illustration of the mRNA-chemical interaction network. Red circles represent mRNA, while purple circles symbolize small molecular compounds.

associated with the MDA content. In Fig. 12C, a reduced GSH concentration can be observed, leading to an impaired redox response in the lung tissue of the Neu group. Additionally, it was found that the mRNA expression of GPX4 decreased in the lung tissue of the Neu group (Fig. 12D). The western blotting detection (Fig. 12E and F) was consistent with the qPCR results. Further investigations were carried out on the expression of HO-1 and HIF-1α proteins in the HIF-1 signaling pathway. It was found that there was a significant increase in HIF-1α and HO-1 protein levels in neutrophilic asthmatic mice (Fig. 12E and H) compared with the control group. Therefore, it can be concluded that the HIF-1 signaling pathway may be involved in ferroptosis during the pathogenesis of neutrophilic asthma. The results were consistent with the biological information analysis.

Discussion

Ferroptosis is considered a special form of cell death that is closely associated with inflammatory diseases (53,54). Unfortunately, understanding of the role of ferroptosis in neutrophilic airway inflammation is still limited. Therefore, exploring central mechanisms associated with ferroptosis in neutrophilic asthma would be of great importance.

The present study focused on the transcriptomic analysis and validation of key genes and biological pathway associated with ferroptosis in neutrophilic asthma. It first created an asthmatic mouse model with neutrophilic airway inflammation using OVA and CFA. The mouse model with the characteristics of neutrophilic airway inflammation (including airway hyperresponsiveness, infiltration of neutrophils and inflammatory cells around the airway and hypersecretion of IL-17A and IFN-γ), demonstrating the mouse model of neutrophilic asthma was successfully constructed. DE-FRGs were then picked out in different models of neutrophilic asthma. Furthermore, KEGG enrichment in three datasets showed that these DE-FRGs were enriched in ferroptosis, HIF-1, NOD-like receptor and IL-17 signaling pathways. In addition, the Pathview analysis of GSE143303 and RNA-seq dataset showed that HIF-1 may have an important influence on ferroptosis by modulation of HMOX1. Simultaneously, 11 common DE-FRGs were screened in neutrophilic asthmatic mice by intersecting the transcriptome dataset with those from the GSE108417 dataset. The key DE-FRGs were then

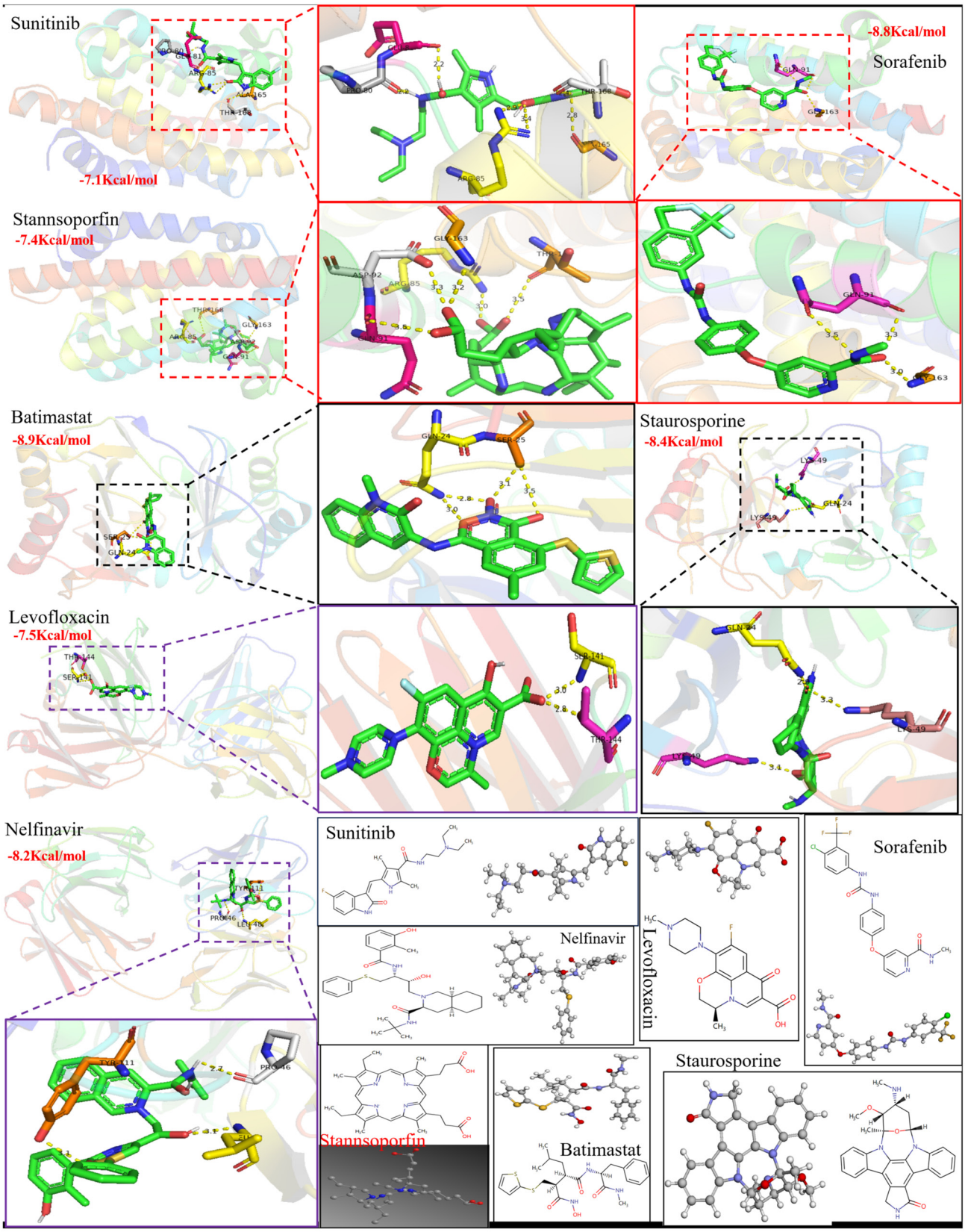

Figure 11. Docking pose of potential therapeutic agents to the correspondingly primary protein in neutrophilic asthma. The 2D/3D structure diagrams of seven candidate molecule drugs and their intermolecular interaction with correspondingly primary protein with a lower affinity of ≤-7 Kcal/mol in neutrophilic asthma. Hydrogen bonds are displayed in yellow dashed lines and green refers to residues at the junction sites.

identified using the PPI analysis. Of these, five key DE-FRGs (IL6, HMOX1, CXCL2, SLC7A5 and TNFAIP3) with good diagnostic value differed markedly in the validation set. To further validate the bioinformatic analysis, the expression levels of these five key genes were further analyzed by qPCR in mouse lung tissues. Among them, IL6, HMOX1, CXCL2

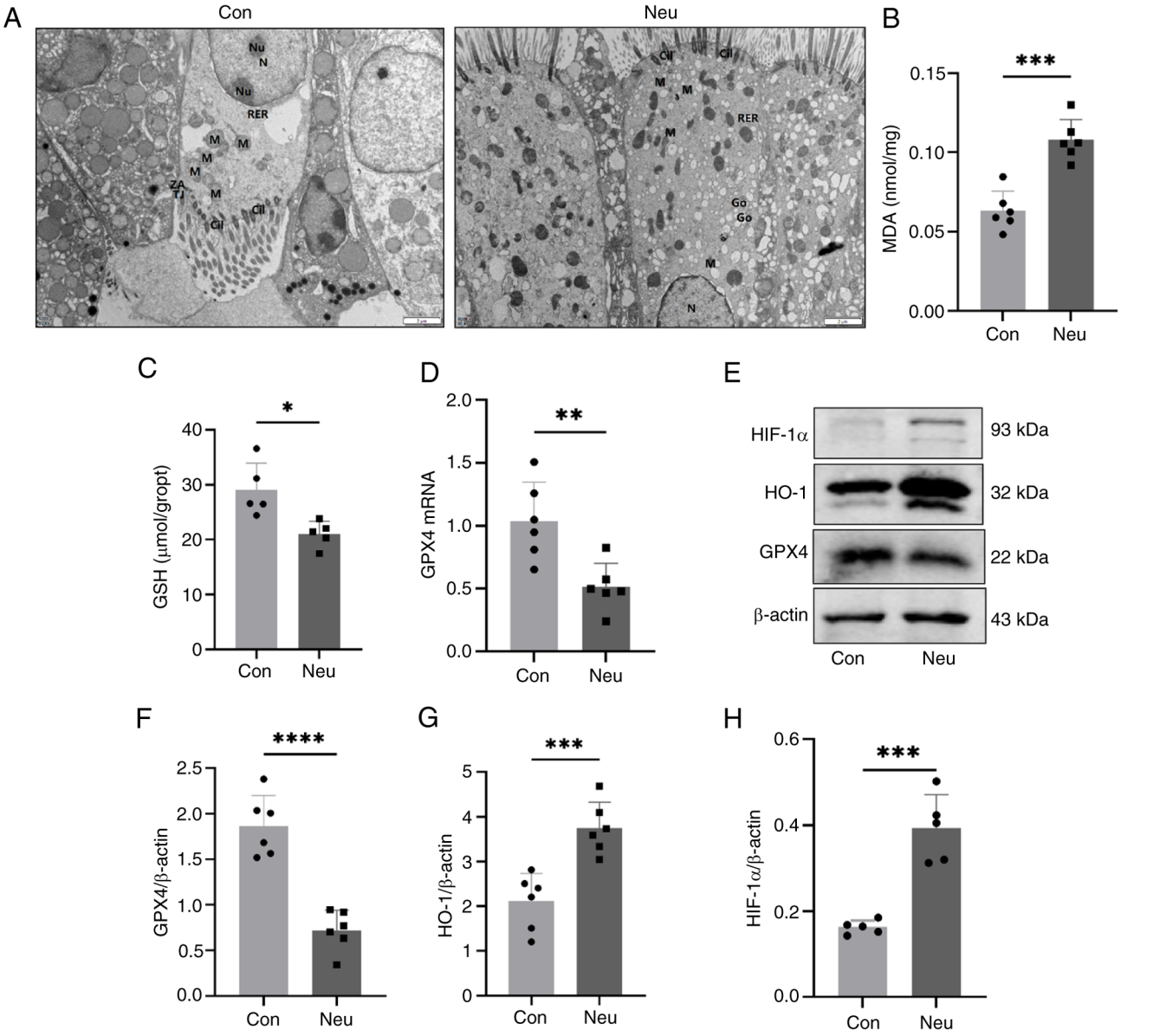

Figure 12. HIF-1 pathway is involved in the ferroptosis of neutrophilic asthma. (A) Transmission electron microscopy images (Scale bar, 2 μm). mRNA expression of (B) MDA, (C) GSH and (D) GPX4; (E-H) GPX4 and proteins associated with the HIF-1α/HO-1 pathway in mice lung tissue (*P<0.05, **P<0.01 ***P<0.005 and ****P<0.001). MDA, malondialdehyde; GSH, glutathione; GPX4, glutathione peroxidase; Mi, mitochondria; N, nucleus; Cil, Cilia; HIF-1, hypoxia-inducible factor 1; HO-1, heme oxygenase 1.

and SLC7A5 were upregulated in the neutrophilic model, which was consistent with the bioinformatics analysis.

Previous studies have shown that these key ferroptosis genes play an important role in the process of ferroptosis. IL-6 was found to be involved in angiotensin II-induced ferroptosis (55). Zhang *et al* (56) emphasized that ferroptosis development in cardiac tissues of hypertensive mice is associated with the IL-6/STAT3 signaling pathway. Other research showed that IL-6 can exacerbate airway inflammation by promoting ROS expression and lipid peroxidation and disrupting cellular iron homeostasis, leading to ferroptosis in bronchial epithelial cells (57). For CXCL2, Yi *et al* (58) have demonstrated that overexpression of CXCL2 is strongly associated with raised expression levels of ROS, Fe^{2+} and MDA in hepatocytes. Inhibition of CXCL2 expression has been shown to reverse the reduced expression of GPX4, diminish ROS production and decrease lipid peroxidation (58). Jin *et al* (59) found that the ferroptosis inducer RLS3 can boost CXCL2 expression induced by HHP. A similar change can be observed in the lung tissue of our engineered asthmatic mice where CXCL2 mRNA levels were markedly increased. Several studies have focused on the association between SLC7A5 and airway inflammation. Inhibition of SLC7A5 expression can inhibit IL-17 production and neutrophil infiltration by interfering with the incorporation of large neutral amino acids (60). SLC7A5 was expected to be a new target for the treatment of Th17-mediated and steroid-resistant severe asthma (60). Furthermore, there is a positive relationship between SLC7A5 level and HIF-1α (61). Consistent with previous studies, the results of the present study also identified SLC7A5 as an important DE-FRG with increased expression in the Neu group. Additionally, HO-1, as a rate-limiting enzyme for heme metabolism (62), is not only

an anti-inflammatory protective factor but also a fundamental regulator of ferroptosis. HO-1-derived iron can increase intracellular lipid peroxidation and lead to ferroptosis. Previous research has shown that high levels of HO-1 expression in doxorubicin-stimulated cardiac tissue are linked to iron deposition in cardiac mitochondria (63). Tang *et al* (64) also reported that excessive activation of HO-1 induces the accumulation of ferrous ions in retinal pigment epithelium (RPE) cells, thereby triggering ferroptosis. By contrast, inhibition of HO-1 expression could effectively prevent RPE ferroptosis. In the present study, the expression level of HO-1 increased in the lung tissue of neutrophilic asthmatic mice. Immune infiltration analysis also indicated that HO-1 was linked to various immune cells, which was consistent with previous studies (65).

Based on the aforementioned analysis, Cytoscape was used to construct mRNA-TF and ceRNA networks and eight TFs, 66 miRNA and 75 lncRNA were predicted that could regulate DE-FRGs providing a direction for the research of transcription and ceRNA post-transcriptional regulatory mechanism of these genes. Simultaneously, the DSigDB database was applied to further predict potential therapeutic agents of key DE-FRGs. As consequence, 35 potential therapeutic drugs were identified. Through molecular docking simulation, small molecule drugs targeting HMOX1, CXCL2, IL6 and SLC7A5 with anti-inflammatory effects were further studied to elucidate interaction mechanism between ferroptosis-related signaling pathway proteins and target drug prediction. A total of 13 small-molecule drugs exhibited higher binding stability with a binding affinity energy of ≤-6 Kcal/mol. Further investigation revealed that seven of the 13 small-molecule drugs had conformations that bind to the corresponding target protein [heme oxygenase 1 (HMOX1), chemokine ligand 2 (CXCL2) and IL6] with a binding affinity energy of ≤-7 Kcal/mol. It was found that the most common interaction residues of HMOX1 and CXCL2 with potential therapeutic drugs were Gln91, Gly163 and Gln24, respectively. This provides a new direction for drug selection in neutrophilic asthma targeting ferroptosis.

The potential mechanism of ferroptosis in neutrophilic asthma was further explored. First, the expression of the ferroptosis signature gene GPX4 and the concentrations of MDA and GSH were detected in mice. GPX4 has an important effect in inhibiting lipid peroxidation by reducing phospholipid hydroperoxides. Reduced expression of GPX4 is a hallmark of ferroptosis (66). It was found that the expression of GPX4 in the lung tissue of mice with neutrophilic asthma was lower compared with that of the Con group. Simultaneously, lipid peroxidation and oxidative stress occurred in the Neu group. It was demonstrated that ferroptosis occurred in the lung tissue of mice with neutrophilic asthma. Next, the enriched signaling pathways of ferroptosis-related genes was examined to understand the potential regulatory mechanisms of ferroptosis in neutrophilic asthma. According to the enrichment analysis, DE-FRGs were mainly enriched in ferroptosis, HIF-1, IL-17 and the NOD-like receptor pathway. Among them, previous studies have shown that HIF-1, as an important factor regulating the hypoxic response (67), was shown to transcriptionally regulates the expression of the ferroptosis gene HMOX1 (68). Moreover, other studies have demonstrated that the HIF-1 signaling pathway is involved in the regulation of ferroptosis. Wu *et al* (69) indicated that DEHP exposure induces ferroptosis in mouse testicular tissues via the HIF-1α/HO-1 pathway. Additionally, Feng *et al* (70) also reported that ferroptosis can exacerbate DN-induced tubular injury via the HIF-1α/HO-1 pathway. Based on the increased HIF-1α expression in the bronchial fluid and lung tissue of asthmatics, as well as in the nasal fluid of rhinitis patients, it can be proven that HIF-1 is directly involved in the development of asthma (71). However, HIF-1α expression as well as its regulatory mechanism in neutrophilic asthma remains unclear and whether it is involved in the occurrence of ferroptosis in neutrophilic asthma remains to be elucidated. Therefore, through bioinformatics analysis combined with experimental validation, it was found that the protein levels of HO-1 and HIF-1α were increased in asthmatic lung tissue, which is closely associated with ferroptosis. It was hypothesized that HIF-1α may play an important role in the progression of ferroptosis in neutrophilic asthma by regulating the transcription of HMOX1. These results shed new light on the role of ferroptosis in the treatment of neutrophilic asthma.

The present study also had some limitations. First, it only use animal models to verify these ferroptosis-related genes. More clinical samples will be needed in the future to further test the hypothesis. Second, although the present study clarified the expression of signature genes and the HIF pathway of ferroptosis in neutrophilic asthma, their role in neutrophilic asthma and the underlying regulatory mechanism are not yet clear. In the future, in-depth studies will be conducted to explore the regulatory role of HIF-1α/HO-1 pathway proteins in ferroptosis of neutrophilic asthma and the mechanism of interaction between pathway proteins to further elucidate the pathogenesis of neutrophilic asthma. It is worth considering that clinical samples for future work could be used to further verify these ferroptosis-related genes as markers or targets in the diagnosis or treatment of neutrophilic asthma.

Collectively, the present study provided evidence for the occurrence of ferroptosis in neutrophilic asthma and used bioinformatic methods to discover FRGs associated with neutrophilic asthma. These genes exhibited good diagnostic value and their expression was markedly different from that of eosinophilic asthma. The results of the present study suggested that the four hub DE-FRGs and the HIF-1 signaling pathway was closely associated with ferroptosis pathogenesis in neutrophilic asthma. The present study provided a novel insight into understanding the pathogenesis of neutrophilic asthma. The identified four hub DE-FRGs and HIF-1 signaling pathway may be proposed as a potential target for the diagnosis or treatment of neutrophilic asthma.

Acknowledgements

Not applicable.

Funding

The present study was approved by Guangxi Natural Science Foundation (approval no. 2020GXNSFDA238003).

Availability of data and materials

Datasets provided in the present work are available from the Gene Expression Omnibus (GEO) database (https://www.ncbi.

nlm.nih.gov/geo/). The raw sequence data reported in this paper have been deposited in the Genome Sequence Archive (72) in National Genomics Data Center (73), China National Center for Bioinformation/Beijing Institute of Genomics, Chinese Academy of Sciences (GSA: CRA015119) that are publicly accessible at https://ngdc.cncb.ac.cn/gsa.

Authors' contributions

CL contributed to the conception and design of the present study. LL and ZL performed bioinformatics analyses and interpreted the results, and wrote the manuscript. SP and SW supervised the experiments and performed the construction of the asthma mouse model. LL, YL and QXS analyzed the database, prepared the diagrams and revised the article. YL and QXS confirm the authenticity of all the raw data. All authors have read and approved the final manuscript.

Ethics approval and consent to participate

Animal experiments were approved by the Ethics Committee of Guangxi Medical University (approval no. 202210101).

Patient consent for publication

Not applicable.

Competing interests

The authors declare that they have no competing interests.

References

1. Hammad H and Lambrecht BN: The basic immunology of asthma. Cell 184: 1469-1485, 2021.
2. Ray A and Kolls JK: Neutrophilic inflammation in asthma and association with disease severity. Trends Immunol 38: 942-954, 2017.
3. Zhao L, Gao J, Chen G, Huang C, Kong W, Feng Y and Zhen G: Mitochondria dysfunction in airway epithelial cells is associated with type 2-low asthma. Front Genet 14: 1186317, 2023.
4. Doe C, Bafadhel M, Siddiqui S, Desai D, Mistry V, Rugman P, McCormick M, Woods J, May R, Sleeman MA, *et al*: Expression of the T helper 17-associated cytokines IL-17A and IL-17F in asthma and COPD. Chest 138: 1140-1147, 2010.
5. Green RH, Brightling CE, Woltmann G, Parker D, Wardlaw AJ and Pavord ID: Analysis of induced sputum in adults with asthma: Identification of subgroup with isolated sputum neutrophilia and poor response to inhaled corticosteroids. Thorax 57: 875-789, 2002.
6. Dixon SJ, Lemberg KM, Lamprecht MR, Skouta R, Zaitsev EM, Gleason CE, Patel DN, Bauer AJ, Cantley AM, Yang WS, *et al*: Ferroptosis: An iron-dependent form of nonapoptotic cell death. Cell 149: 1060-1072, 2012.
7. Jiang YH, Wu SY, Wang Z, Zhang L, Zhang J, Li Y, Liu C, Wu WZ and Xue YT: Bioinformatics analysis identifies ferroptosis-related genes in the regulatory mechanism of myocardial infarction. Exp Ther Med 24: 748, 2022.
8. Shao L, Fang Q, Ba C, Zhang Y, Shi C, Zhang Y and Wang J: Identification of ferroptosis-associated genes in chronic kidney disease. Exp Ther Med 25: 60, 2022.
9. Hu T, Yu WP, Zou HX, Chai ZH, Le SY, Hu FJ, Wang YC, Huang H, Lai SQ and Liu JC: Role of dysregulated ferroptosis-related genes in cardiomyocyte ischemia-reperfusion injury: Experimental verification and bioinformatics analysis. Exp Ther Med 26: 534, 2023.
10. Zhou Q, Li T, Qin Q, Huang X and Wang Y: Ferroptosis in lymphoma: Emerging mechanisms and a novel therapeutic approach. Front Genet 13: 1039951, 2022.
11. Wang Q, Xiong Z, Wang B, Wang W and Zheng H: Ferroptosis and preeclampsia: Genetic analysis of potential biomarkers and therapeutic targets. Biochem Genet 62: 853-875, 2024.
12. Tang W, Dong M, Teng FZ, Cui J, Zhu X, Wang W, Wuniqiemu T, Qin J, Yi L, Wang S, *et al*: Environmental allergens house dust mite-induced asthma is associated with ferroptosis in the lungs. Exp Ther Med 22: 1483, 2021.
13. Yang N and Shang Y: Ferrostatin-1 and 3-methyladenine ameliorate ferroptosis in OVA-induced asthma model and in IL-13-challenged BEAS-2B cells. Oxid Med Cell Longev 2022: 9657933, 2022.
14. Bao C, Liu C, Liu Q, Hua L, Hu J, Li Z and Xu S: Liproxstatin-1 alleviates LPS/IL-13-induced bronchial epithelial cell injury and neutrophilic asthma in mice by inhibiting ferroptosis. Int Immunopharmacol 109: 108770, 2022.
15. Zhao X, Gao S, Ren H, Sun W, Zhang H, Sun J, Yang S and Hao J: Hypoxia-inducible factor-1 promotes pancreatic ductal adenocarcinoma invasion and metastasis by activating transcription of the actin-bundling protein fascin. Cancer Res 74: 2455-2464, 2014.
16. Gui D, Li Y, Chen X, Gao D, Yang Y and Li X: HIF-1 signaling pathway involving iNOS, COX-2 and caspase-9 mediates the neuroprotection provided by erythropoietin in the retina of chronic ocular hypertension rats. Mol Med Rep 11: 1490-1496, 2015.
17. Fu X and Zhang F: Role of the HIF-1 signaling pathway in chronic obstructive pulmonary disease. Exp Ther Med 16: 4553-4561, 2018.
18. Dong H, Zhang C, Shi D, Xiao X, Chen X, Zeng Y, Li X and Xie R: Ferroptosis related genes participate in the pathogenesis of spinal cord injury via HIF-1 signaling pathway. Brain Res Bull 192: 192-202, 2023.
19. Qian JW, Wang C, Wang B, Yang J, Wang Y, Luo F, Xu J, Zhao C, Liu R and Chu Y: The IFN-γ/PD-L1 axis between T cells and tumor microenvironment: Hints for glioma anti-PD-1/PD-L1 therapy. J Neuroinflamm 15: 290, 2018.
20. Chen L, Hou W, Liu F, Zhu R, Lv A, Quan W and Mao S: Blockade of NLRP3/caspase-1/IL-1β regulated Th17/treg immune imbalance and attenuated the neutrophilic airway inflammation in an ovalbumin-induced murine model of asthma. J Immunol Res 2022: 9444227, 2022.
21. Bogaert P, Naessens T, De Koker S, Hennuy B, Hacha J, Smet M, Cataldo D, Di Valentin E, Piette J, Tournoy KG and Grooten J: Inflammatory signatures for eosinophilic vs neutrophilic allergic pulmonary inflammation reveal critical regulatory checkpoints. Am J Physiol Lung Cell Mol Physiol 300: L679-L690, 2011.
22. Chen X, Jiang X, Lu Y, Yao Y, Lu J, Zhi Q, Lai L, Liang J and Li C: Aerosol inhalation of Mycobacterium bovis can reduce the Th2 dominant immune response induced by ovalbumin sensitization. Am J Transl Res 14: 3430-3438, 2022.
23. Li L, Sun Q, Xiao H, Zhang Q, Xu S, Lai L, Li Z and Li C: Aerosol inhalation of heat-killed clostridium butyricum CGMCC0313-1 alleviates allergic airway inflammation in mice. J Immunol Res 2022: 8447603, 2022.
24. Xiao H, Zhang QN, Sun QX, Li LD, Xu SY and Li CQ: Transcriptomic analysis reveals a link between hippo signaling pathway and macrophages in lungs of mice with OVA-induced allergic asthma. J Inflamm Res 15: 423-437, 2022.
25. Dong L, Wang Y, Zheng T, Pu Y, Ma Y, Qi X, Zhang W, Xue F, Shan Z, Liu J, *et al*: Hypoxic hUCMSC-derived extracellular vesicles attenuate allergic airway inflammation and airway remodeling in chronic asthma mice. Stem Cell Res Ther 12: 4, 2021.
26. Jia M, Fu H, Jiang X, Wang L, Xu J, Barnes PJ, Adcock IM, Liu Y, He S, Zhang F, *et al*: DEL-1, as an anti-neutrophil transepithelial migration molecule, inhibits airway neutrophilic inflammation in asthma. Allergy 79: 1180-1194, 2024.
27. Pertea M, Pertea GM, Antonescu CM, Chang TC, Mendell JT and Salzberg SL: StringTie enables improved reconstruction of a transcriptome from RNA-seq reads. Nat Biotechnol 33: 290-295, 2015.
28. Pertea M, Kim D, Pertea GM, Leek JT and Salzberg SL: Transcript-level expression analysis of RNA-seq experiments with HISAT, StringTie and ballgown. Nat Protoc 11: 1650-1667, 2016.
29. Love MI, Huber W and Anders S: Moderated estimation of fold change and dispersion for RNA-seq data with DESeq2. Genome Biol 15: 550, 2014.
30. Subramanian A, Tamayo P, Mootha VK, Mukherjee S, Ebert BL, Gillette MA, Paulovich A, Pomeroy SL, Golub TR, Lander ES and Mesirov JP: Gene set enrichment analysis: A knowledge-based approach for interpreting genome-wide expression profiles. Proc Natl Acad Sci USA 102: 15545-15550, 2005.

31. Ogata H, Goto S, Sato K, Fujibuchi W, Bono H and Kanehisa M: KEGG: Kyoto encyclopedia of genes and genomes. Nucleic Acids Res 27: 29-34, 1999.
32. Dusa A: venn: Draw Venn Diagrams R package. R Core Team, Vienna, 2020.
33. von Mering C, Huynen M, Jaeggi D, Schmidt S, Bork P and Snel B: STRING: A database of predicted functional associations between proteins. Nucleic Acids Res 31: 258-261, 2003.
34. Ritchie ME, Phipson B, Wu D, Hu Y, Law CW, Shi W and Smyth GK: limma powers differential expression analyses for RNA-sequencing and microarray studies. Nucleic Acids Res 43: e47, 2015.
35. Kassambara A: ggpubr: 'ggplot2' based publication ready plots. R package version 0.4. 0, 2020. https://CRAN.R-project.org/package=ggpubr.
36. Robin X, Turck N, Hainard A, Tiberti N, Lisacek F, Sanchez JC and Müller M: pROC: An open-source package for R and S+ to analyze and compare ROC curves. BMC Bioinformatics 12: 77, 2011.
37. Ginestet C: ggplot2: Elegant graphics for data analysis. J R Stat Soc Ser A 174: 245-245, 2011.
38. Smoot ME, Ono K, Ruscheinski J, Wang PL and Ideker T: Cytoscape 2.8: New features for data integration and network visualization. Bioinformatics 27: 431-432, 2011.
39. Wong N and Wang X: miRDB: An online resource for microRNA target prediction and functional annotations. Nucleic Acids Res 43 (Database Issue): D146-D152, 2015.
40. Dweep H, Sticht C, Pandey P and Gretz N: miRWalk-database: Prediction of possible miRNA binding sites by 'walking' the genes of three genomes. J Biomed Inform 44: 839-847, 2011.
41. Furió-Tarí P, Tarazona S, Gabaldón T, Enright AJ and Conesa A: spongeScan: A web for detecting microRNA binding elements in lncRNA sequences. Nucleic Acids Res 44 (W1): W176-W180, 2016.
42. Yoo M, Shin J, Kim J, Ryall KA, Lee K, Lee S, Jeon M, Kang J and Tan AC: DSigDB: Drug signatures database for gene set analysis. Bioinformatics 31: 3069-3071, 2015.
43. Morris GM, Goodsell DS, Halliday RS, Huey R, Hart WE, Belew RK and Olson AJ: Automated docking using a Lamarckian genetic algorithm and an empirical binding free energy function. J Comput Chem 19: 1639-1662, 1998.
44. Wishart DS, Feunang YD, Guo AC, Lo EJ, Marcu A, Grant JR, Sajed T, Johnson D, Li C, Sayeeda Z, *et al*: DrugBank 5.0: A major update to the DrugBank database for 2018. Nucleic Acids Res 46 (D1): D1074-D1082, 2018.
45. Berman HM, Westbrook J, Feng Z, Gilliland G, Bhat TN, Weissig H, Shindyalov IN and Bourne PE: The protein data bank. Nucleic Acids Res 28: 235-242, 2000.
46. Tian YN, Zhou YH, Li L, Huang C, Lin L, Li C and Ye Y: Effect of substrate composition on physicochemical properties of the medium-long-medium structured triacylglycerol. J Sci Food Agric 104: 942-955, 2023.
47. Livak KJ and Schmittgen TD: Analysis of relative gene expression data using real-time quantitative PCR and the 2(-Delta Delta C(T)) method. Methods 25: 402-408, 2001.
48. Raundhal M, Morse C, Khare A, Oriss TB, Milosevic J, Trudeau J, Huff R, Pilewski J, Holguin F, Kolls J, *et al*: High IFN-γ and low SLPI mark severe asthma in mice and humans. J Clin Invest 125: 3037-3050, 2015.
49. McKinley L, Alcorn JF, Peterson A, Dupont RB, Kapadia S, Logar A, Henry A, Irvin CG, Piganelli JD, Ray A and Kolls JK: TH17 cells mediate steroid-resistant airway inflammation and airway hyperresponsiveness in mice. J Immunol 181: 4089-4097, 2008.
50. Zeng Z, Huang H, Zhang J, Liu Y, Zhong W, Chen W, Lu Y, Qiao Y, Zhao H, Meng X, *et al*: HDM induce airway epithelial cell ferroptosis and promote inflammation by activating ferritinophagy in asthma. FASEB J 36: e22359, 2022.
51. Deng B, Liao F, Liu Y, He P, Wei S, Liu C and Dong W: Comprehensive analysis of endoplasmic reticulum stress-associated genes signature of ulcerative colitis. Front Immunol 14: 1158648, 2023.
52. Choi W, Wu Y, Li Y and Dong J: Network pharmacology prediction and molecular docking analysis reveal the mechanism of modified Bushen Yiqi formulas on chronic obstructive pulmonary disease. J Gene Med 26: e3607, 2024.
53. Cao F, Luo A and Yang C: G6PD inhibits ferroptosis in hepatocellular carcinoma by targeting cytochrome P450 oxidoreductase. Cell Signal 87: 110098, 2021.
54. Wang S, Song Y, Xu F, Liu H, Shen Y, Hu L, Fu Y and Zhu L: Identification and validation of ferroptosis-related genes in lipopolysaccharide-induced acute lung injury. Cell Signal 108: 110698, 2023.
55. Chen D, Li Z, Bao P, Chen M, Zhang M, Yan F, Xu Y, Ji C, Hu X, Sanchis D, *et al*: Nrf2 deficiency aggravates angiotensin II-induced cardiac injury by increasing hypertrophy and enhancing IL-6/STAT3-dependent inflammation. Biochim Biophys Acta Mol Basis Dis 1865: 1253-1264, 2019.
56. Zhang Z, Tang J, Song J, Xie M, Liu Y, Dong Z, Liu X, Li X, Zhang M, Chen Y, *et al*: Elabela alleviates ferroptosis, myocardial remodeling, fibrosis and heart dysfunction in hypertensive mice by modulating the IL-6/STAT3/GPX4 signaling. Free Radical Bio Med 181: 130-142, 2022.
57. Han F, Li S, Yang Y and Bai Z: Interleukin-6 promotes ferroptosis in bronchial epithelial cells by inducing reactive oxygen species-dependent lipid peroxidation and disrupting iron homeostasis. Bioengineered 12: 5279-5288, 2021.
58. Yi Q, Liang Q, Liu Y, Gong Z and Yan Y: Application of genomic selection and experimental techniques to predict cell death and immunotherapeutic efficacy of ferroptosis-related CXCL2 in hepatocellular carcinoma. Front Oncol 12: 998736, 2022.
59. Jin R, Yang R, Cui C, Zhang H, Cai J, Geng B and Chen Z: Ferroptosis due to cystathionine γ Lyase/hydrogen sulfide down-regulation under high hydrostatic pressure exacerbates VSMC dysfunction. Front Cell Dev Biol 10: 829316, 2022.
60. Hayashi K, Saeki M, Miura K, Yamasaki N, Matsuda M, Shimora H, Nabe T, Shimizu Y, Fujita T, Endou H and Kaminuma O: JPH203, a LAT1 inhibitor, alleviates steroid-resistant murine airway inflammation mediated by Th17 cells. Allergy 78: 2780-2783, 2023.
61. Törnroos R, Tina E and Eremo AG: SLC7A5 is linked to increased expression of genes related to proliferation and hypoxia in estrogen-receptor-positive breast cancer. Oncol Rep 47: 17, 2022.
62. Consoli V, Sorrenti V, Grosso S and Vanella L: Heme oxygenase-1 signaling and redox homeostasis in physiopathological conditions. Biomolecules 11: 589, 2021.
63. Kwon MY, Park E, Lee SJ and Chung SW: Heme oxygenase-1 accelerates erastin-induced ferroptotic cell death. Oncotarget 6: 24393-24403, 2015.
64. Tang Z, Ju Y, Dai X, Ni N, Liu Y, Zhang D, Gao H, Sun H, Zhang J and Gu P: HO-1-mediated ferroptosis as a target for protection against retinal pigment epithelium degeneration. Redox Bio 43: 101971, 2021.
65. Wong TH, Chen HA, Gau RJ, Yen JH and Suen JL: Heme oxygenase-1-expressing dendritic cells promote Foxp3+ regulatory T cell differentiation and induce less severe airway inflammation in murine models. PLoS One 11: e0168919, 2016.
66. Feng FH, He SS, Li XL, He JK and Luo LX: Mitochondria-mediated ferroptosis in diseases therapy: From molecular mechanisms to implications. Aging Dis 15: 714-738, 2024.
67. McGettrick AF and O'Neill LAJ: The role of HIF in immunity and inflammation. Cell Metab 32: 524-536, 2020.
68. Zhongyin Z, Wei W, Juan X and Guohua F: Isoliquiritin apioside relieves intestinal ischemia/reperfusion-induced acute lung injury by blocking Hif-1α-mediated ferroptosis. Int Immunopharmacol 108: 108852, 2022.
69. Wu Y, Wang J, Zhao T, Chen J, Kang L, Wei Y, Han L, Shen L, Long C, Wu S and Wei G: Di-(2-ethylhexyl) phthalate exposure leads to ferroptosis via the HIF-1α/HO-1 signaling pathway in mouse testes. J Hazard Mater 426: 127807, 2022.
70. Feng X, Wang S, Sun Z, Dong H, Yu H, Huang M and Gao X: Ferroptosis enhanced diabetic renal tubular injury via HIF-1α/HO-1 Pathway in db/db mice. Front Endocrinol (Lausanne) 12: 526390, 2021.
71. Huerta-Yepez S, Baay-Guzman GJ, Bebenek IG, Hernandez-Pando R, Vega MI, Chi L, Riedl M, Diaz-Sanchez D, Kleerup E, Tashkin DP, *et al*: Hypoxia inducible factor promotes murine allergic airway inflammation and is increased in asthma and rhinitis. Allergy 66: 909-918, 2011.
72. Chen T, Chen X, Zhang S, Zhu J, Tang B, Wang A, Dong L, Zhang Z, Yu C, Sun Y, *et al*: The genome sequence archive family: Toward explosive data growth and diverse data types. Genomics Proteomics Bioinformatics 19: 578-583, 2021.
73. National Genomics Data Center Members and Partners: Database resources of the national genomics data center in 2020. Nucleic Acids Res 48 (D1): D24-D33, 2020.